Cell Division Drives Epithelial Cell Rearrangements during Gastrulation in Chick

Joao Firmino, Didier Rocancourt, Mehdi Saadaoui, Chloé Moreau, Jerome Gros

Cell Division Drives Epithelial Cell Rearrangements during Gastrulation in Chick

Joao Firmino[1,2*], Didier Rocancourt[1,2*], Mehdi Saadaoui[1,2], Chloe Moreau[1,2,3] and Jerome Gros[1,2†]

[1]Department of Developmental and Stem Cell Biology
Institut Pasteur
25 rue du Docteur Roux, 75724 Paris, Cedex 15, France

[2] CNRS URA2578,
rue du Dr Roux, 75015 Paris, France

[3] Univ. Pierre et Marie Curie, Cellule Pasteur UPMC,
rue du Dr Roux, 75015 Paris, France

*These authors contributed equally to this work.

† To whom correspondence should be addressed:
Phone: +33 (0)1-45-68-81-45
Email: jgros@pasteur.fr

Summary

During early embryonic development, cells are organized as cohesive epithelial sheets that are continuously growing and remodeled without losing their integrity, giving rise to a wide array of tissue shapes. Here, using live imaging in chick embryo, we investigate how epithelial cells rearrange during gastrulation. We find that cell division is a major rearrangement driver that powers dramatic epithelial cell intercalation events. We show that these cell division mediated intercalations, which represent the majority of epithelial rearrangements within the early embryo, are absolutely necessary for the spatial patterning of gastrulation movements. Furthermore, we demonstrate that these intercalation events result from overall low cortical actomyosin accumulation within the epithelial cells of the embryo, which enables dividing cells to remodel junctions in their vicinity. These findings uncover a previously unappreciated role for cell division as coordinator of epithelial growth and remodeling that might underlie various developmental, homeostatic or pathological processes in amniotes.

Introduction

During embryonic development, gastrulation is the first major morphogenetic event that leads to the formation of the three embryonic layers (i.e. ectoderm, mesoderm and endoderm). In chick, gastrulation involves large-scale cellular movements, taking place within the single-celled layer epithelial embryo. These cell movements first described in 1929 (Gräper, 1929; Wetzel, 1929) were named 'Polonaise movements' due to their resemblance to a Polish dance choreography: upon incubation, within the flat epiblast disk, two counter rotational flows of cells merge at the posterior end of the embryonic disk to form the primitive streak (i.e. site of mesendoderm formation and future midline of the embryo). More recently, it has been shown that the primitive streak progressively forms and elongates through cell shape changes, mediolateral intercalation and ingression of epithelial cells at the posterior margin of the epiblast (Rozbicki et al., 2015; Voiculescu et al., 2007, 2014). Whereas such cell-cell interactions have been elegantly demonstrated to drive streak elongation, they do not however provide, on their own, a plausible explanation for the circular flows of cells concomitantly observed in the epiblast. In their models Voiculescu et al. and Rozbicki et al., propose that the cell displacements induced by shape changes, ingressions and intercalations at the streak are "propagated" throughout the epiblast. These peculiar cell movements taking place in the epithelial embryo, in which cells are connected by adherens junctions, pose a conceptual problem: How can movements be propagated within the rapidly growing epiblast without disrupting the epithelial integrity of the embryo? Do cells rearrange within the epiblast or exhibit specific behaviors participating to the spatial patterning of gastrulation movements? If so what are the underlying cellular and molecular mechanisms?

Epithelial rearrangement events have been extensively characterized in invertebrates, in particular *Drosophila*. In this model, a number of stereotyped key events (for review see (Guillot and Lecuit, 2013a), have been identified. During germband elongation in *Drosophila*, an ordered process of cell intercalation such as T1 processes (involving 4 cells) (Bertet et al., 2004), and the formation/resolution of rosettes (involving 5 cells or more) (Blankenship et al., 2006) underlies the elongation of the embryo: epithelial cells undergo planar

polarized remodeling of junctions driven by a myosin-dependent junction shortening in one plane, followed by lengthening in the perpendicular plane. Epithelial cells have also been shown to rearrange through T2 processes, during which junctions are removed by a cell extrusion mechanism, as observed in the *Drosophila* notum (Marinari et al., 2012).

During all the above-mentioned processes cells do not divide. The process of cell division has been shown to play important roles in epithelial tissue morphogenesis in zebrafish and *Drosophila*, in particular through polarized orientation which can be instructed by signaling pathways (Baena-López et al., 2005; Gong et al., 2004; Saburi et al., 2008, for review see Morin and Bellaïche, 2011) or in response to mechanical stress (Campinho et al., 2013; LeGoff et al., 2013; Mao et al., 2013; Wyatt et al., 2015). However, cell division itself does not directly promote rearrangements of epithelial cells: upon cell division, it has been reported that daughter cells almost always share a common interface and do not intercalate between their neighbors (Bischoff and Cseresnyés, 2009; Gibson et al., 2006). Aside from the addition of a novel cell-cell junction at the interface between the two daughters, the overall junctional organization and therefore the epithelial topology remains globally unchanged. This is exemplified by numerous clonal analyses performed in *Drosophila* in which clonal descendants remain compact and do not disperse within the epithelial tissue (Knox and Brown, 2002). Recently, the mechanisms underlying the formation of a new daughter-daughter cell junction have been brought to light. Studies performed in the *Drosophila* early embryonic and pupal notum epithelia have shown that cell division can be regarded as a multicellular process involving not only a dividing cell but also its immediate neighbors. These studies show that as cytokinesis takes place, the contractile tension exerted by the cytokinetic ring of a dividing cell is resisted by its neighbors (actomyosin based cortical tension). This ratio of forces at the site of cytokinesis ultimately results in local adhesion disengagement of the dividing cell with its neighbor, the annealing of the two daughter's membrane and the subsequent formation of a new daughter-daughter cell junction (Founounou et al., 2013; Guillot and Lecuit, 2013a; Herszterg et al., 2013). The observation that cell division does not directly promote epithelial cell rearrangements does not appear to be confined to *Drosophila* epithelia but can also be observed in the developing epithelia of *C.elegans*, zebrafish and *Xenopus* (Harrell and

Goldstein, 2011; Kieserman et al., 2008; Olivier et al., 2010) and it has been implied to be a conserved feature among Metazoan (Gibson et al., 2006). Recently, cell division has been observed to be associated with cell dispersal in the mouse ureteric bud (Packard et al., 2013) and with rearrangements during mouse limb ectoderm morphogenesis (Lau et al., 2015). These studies have observed that in mouse, daughter cells do not necessarily share a common interface, questioning the universality of a daughter-daughter cell junction formation upon epithelial cell division in Metazoan. However, these studies did not examine the role of cell division in cell-cell intercalations and in overall epithelial morphogenesis. It thus remains unaddressed whether cell division acts as a regulatory mechanism in epithelial rearrangements and in epithelial morphogenesis in general or whether these rearrangements associated with cell division are only incidental. Importantly, these observations beg the question of the underlying molecular mechanisms that would allow dividing cells to promote rearrangements, as opposed to what has been observed in epithelia of *Drosophila*, *C. elegans*, zebrafish and *Xenopus*.

In this paper, we investigate the cellular mechanisms underlying the spatial patterning of gastrulation movements in chick and the role of cell division in this process. The early chick embryo develops as a flat, highly proliferative epithelial disk that can be easily live-imaged for long periods of time; it is thus an excellent system to study dynamic epithelial rearrangements in an amniote system. Using this model, we find that cell division promotes dramatic rearrangements of epithelial cells and we show that these rearrangements play a critical role in the spatial patterning of gastrulation movements; furthermore we bring evidence that cell-cell intercalations induced by division are the consequence of an interplay between the actomyosin cytoskeleton of dividing cells and the cortical actomyosin of their immediate neighbors that enables dividing cells to remodel junctions in their vicinity.

Results

Cell division is a major epithelial rearrangement driver during gastrulation

Previous studies focused on the cellular events driving primitive streak formation. Here, we decided to investigate whether cells of the epiblast away from the presumptive primitive streak, which actually display the

rotational movements, exhibit specific behaviors that could play a role in the spatial patterning of these characteristic movements. To visualize gastrulation movements, as they are taking place, we electroporated stage X chick embryos (Eyal Giladi-Kochav staging system, 0 hour of incubation) with a Green Fluorescent Protein (GFP) reporter gene and followed the behavior of electroporated cells at stage 3 (Hamburger and Hamilton staging system, around 12-15h of incubation) using the EC culture system (Chapman et al., 2001) and confocal microscopy (10x objective, Figure 1A and Movie S1). Using high resolution (40x objective) confocal microscopy, we unexpectedly observed that at about stage 3, as gastrulation movements are taking place, most daughter cells rapidly separate from each other in regions away from the primitive streak (Figure 1B and Movie S1). This observation is in sharp contrast to what has been previously observed in other epithelia (e.g. in *Drosophila*, *C. elegans*, zebrafish and *Xenopu*s embryos), where daughter cells almost always remain in contact (Bischoff and Cseresnyés, 2009; Campinho et al., 2013; Gibson et al., 2006; Harrell and Goldstein, 2011, Kieserman et al., 2008). Since epiblast cells are connected by adherens junctions of E-Cadherin, we reasoned that neighboring cells must intercalate in between daughter cells in order to maintain epithelial integrity. To verify this, we live imaged transgenic chicken embryos expressing a membrane-bound GFP (memGFP) (Rozbicki et al., 2015) to reveal all cell boundaries within the epiblast from stage X until stage 3+. Large epithelial regions (approximately 5000-10000 cells, $1mm^2$), anterior and lateral to the primitive streak-forming region (at approximately 500μm distance), were imaged and analyzed (see Figure 1C and Movie S2). Interestingly, we found that at stage X, following cell division, most daughter cells remain in direct contact for at least 30min after cytokinesis has completed (90%, n=738; 7 embryos, Figure 1D and E and movie S2). However, as gastrulation movements take place, epithelial cells in contact with a mitotic cell increasingly intercalate in between daughter cells (within 30 min after cytokinesis has completed), reaching 90 % of intercalations at stage 3 (n=530; 5 embryos; referred as Cytokinesis Mediated Intercalation, CMI; Figures 1D, 1F, 1G and Movies S1 and S2). In addition to neighboring cells intercalating in between daughter cells, we noticed that daughter cells themselves also intercalate in between their neighbors (referred as Daughter Cell Associated Intercalation, DCAI; Figure 1F and Movies S1 and S2). Notably, as observed for CMI most division

events promoted DCAI (93%).

We next sought to quantify the proportion of cell division mediated intercalations (including both CMI and DCAI) in relation to other epithelial cell rearrangement events. This was done by analyzing the evolution of every junction within a given region of memGFP transgenic embryos, over a 1h-period at stage 3, as gastrulation movements are taking place (n= 1150 junctions analyzed, 5 embryos; for explanation on how junction states were assigned please refer to experimental procedures and Movie S3). We found that 63% of cell-cell junctions did not remodel (i.e. did not undergo any transitions; referred as "stable"); only 13% of junctions remodeled without involving cell division (i.e. T1 or T2 processes; referred as "T processes") whereas 24% of junctions remodeled involving a cell division event (Cytokinesis Mediated Transitions: 11% and Daughter Cell Associated Transitions: 13%; Figures 2D, D', F and Movie S3). Thus, cell division mediated intercalations account for the vast majority of junctional remodeling events occurring in the highly proliferating epiblast, away from the primitive streak and as gastrulation movements take place.

Cell division mediated intercalations are necessary for the spatial patterning of gastrulation movements

We next investigated the potential role of cell division mediated intercalations in contributing to the spatial patterning of gastrulation movements. Previous studies have shown that inhibition of cell division, strongly affects cell movements during chick gastrulation, a phenotype attributed to a failure of the embryonic tissue to expand through an increase in cell number (Cui et al., 2005). In light of our findings, we decided to re-investigate the effect of the inhibition of cell division on the gastrulation movements and importantly on cell rearrangements. In control GFP-electroporated embryos, the two counter rotational flows of cells continuously take place (Figures 2A-C, 2A'-C' and Movie S1). However, upon Aphidicolin exposure, a potent DNA polymerase inhibitor that indirectly prevents cell division uniformly within the epithelial embryo, movements still occurred but the typical circular pattern was rapidly impaired. At the concentration we used, Aphidicolin induced an 80% decrease in cell division compared to control embryos (as counted per number of dividing

cells/μm^2 per hour, n= 2140 cells, 4 embryos, see experimental procedure for details). Importantly, cells did not display symmetrical rotational movements but instead converged towards the primitive streak (Figures 2G-I, 2G'-I' and Movie S4), confirming previous observations (Cui et al., 2005). These results suggest that cell division does not act as a driving force of gastrulation movements but rather appears to be important for their spatial patterning. We therefore analyzed cell-cell junctions over time in Aphidicolin treated memGFP transgenic embryos to gain insights into the cell rearrangements taking place when cell division is abrogated. Not surprisingly, in this condition cell division mediated intercalation events were almost completely abrogated (1%) (Figures 2J, 2J', 2F and Movie S3). Importantly, 89% of epithelial junctions were stable while only 10% of junctions exhibited cell division independent rearrangements ("T" processes) (n=832 junctions, 4 embryos). Thus, inhibition of cell division "stabilized" epithelial organization over time, which resulted in little cell rearrangements compared to control embryos (Figures 2E, 2E', 2K and 2K' and Movies S3). Notably, very similar results were obtained using Aminopterin, a different compound causing cell division inhibition (89% decrease in cell division, as counted per number of dividing cells/μm^2 per hour, n= 1500 cells, 3 embryos) through thymidylate depletion (Figure 2F and Figure S1). Taken together these data demonstrate that cell division acts as a powerful and major epithelial cell-remodeling driver that enables the continuous cell rearrangements necessary to spatially pattern movements during gastrulation.

Cell division actively promotes epithelial rearrangements

It has recently been described that primitive streak formation which is driven by cell intercalation and ingression is accompanied by the appearance of local directed strains within the epiblast (Rozbicki et al., 2015). Because in other systems, directed strains have been shown to orient cell division to relieve tension within epithelial tissue (Campinho et al., 2013; LeGoff et al., 2013; Mao et al., 2013; Wyatt et al., 2015), we sought out to determine whether daughter cell separation could also be a tension-relieving mechanism and therefore a passive consequence of external forces arising from the primitive streak forming region. First, we determined the timing of daughter cell separation relative to initiation of gastrulation movements. We found that the onset

of daughter cell separation preceded by few hours the appearance of local movements within the epiblast (Figure 1D). Therefore it is very unlikely that local directed strains induced by primitive streak forming region could account for the initiation of daughter cell separation. Second, if daughter cell separation is a consequence of external forces at work within the epiblast, then orientation of cell division (and subsequent intercalations) should be aligned with local tissue movements, as observed in other systems (Campinho et al., 2013; LeGoff et al., 2013; Mao et al., 2013; Wyatt et al., 2015) . We therefore quantified the orientation of cell division in regions of the epiblast away from the primitive streak-forming region and normalized the angles of cell division with respect to the local tissue flow. We could not find any sign of alignment of cell division orientation with the local tissue flow, which appeared largely isotropic (Figures 3A-C and Movie S2, n=390 cells, 3 embryos, χ^2 test, p-value= 0.85), further supporting that external forces do not act to promote daughter cell separation. Finally, to functionally address whether external forces act to separate daughter cells upon division, we used UV laser micro-dissection in stage 3 embryos to isolate epithelial regions of the epiblast, thereby alleviating these regions from primitive streak-induced external forces. Laser micro-dissection efficiently resulted in isolation of epithelial regions (about 1000 cells) from the rest of the embryo, which were then analyzed for 1 h using live imaging microscopy (Figures 3D-E and movie S5). Whereas tissue flow was close to normal outside the isolated regions (i.e. cells displayed rotational movement), tissue flow within isolated regions was abrogated, demonstrating that such isolated regions behave independently of the rest of the embryo and therefore independently of local directed strains arising from the primitive streak-forming region. Importantly, in these isolated regions the proportion of daughter cell separation showed no significant differences compared to stage 3 control embryos (Figure 3F, n=182, 4 embryos). Altogether, these results demonstrate that cell division mediated rearrangements arise from an active process and are not the consequence of external mechanical stimuli. Moreover, these results suggest that such cell behavior is an inherent property of the epithelial embryonic tissue at this stage.

Spatiotemporal characterization of cell division mediated intercalations

Next, we investigated how cell division mediated intercalations are spatiotemporally controlled. Because cell division promotes cellular rearrangements at stage 3 but not at stage X, comparison between these stages can provide clues for mechanisms underlying cell division mediated intercalations. We used high-resolution 4D (x, y, z, t), 2-photon live imaging microscopy on memGFP transgenic embryos to capture a dividing cell and its neighbors in both space and time. At stage 3, we observed that cell division mediated intercalation is a multistep process: First, as the dividing cell rounds up apically, neighboring cells become dramatically deformed and concomitantly establish novel contacts basally; Second, as the cytokinetic ring contracts from basal to apical, the contact between the dividing cell and its neighbors is carried along; Third, this novel cell contact finally expands into a stable cell-cell junction in the plane of the epithelium (Figures S2A, S2A', S2A''). In contrast, at stage X, as cells round up and start dividing, neighbors undergo only very local deformations and stable contacts between originally distant neighbors is not observed basally, instead a daughter-daughter cell junction forms almost immediately (Figures S2B, S2B', S2B"). Furthermore, analysis of junctions at stage X revealed that the epithelium is very "stable" (92%) with few T processes, CMI and DCAI (5%, 2%, 1%, respectively; n=551, 2 embryos) (Figure S2C). These observations suggest that at stage 3 dividing cells are able to dramatically deform and displace neighbors, eventually bringing them into contact in between daughter cells, whereas at stage X cells divide in a highly stable epithelium that might prevent dividing cells from rearranging junctions in their vicinity.

Differences in F-actin and Myosin localization and dynamics underlie cell division mediated rearrangements.

In order for dividing cells to mechanically deform neighbors and displace them, we reasoned that non-dividing epithelial cells must exhibit relatively low cortical rigidity (allowing neighbor deformation) as well as low cell-cell junction stability (allowing planar displacement through junction exchange). Because, at the molecular level, both low cortical rigidity and low E-Cadherin junction stability have been linked to high

actomyosin cytoskeleton turn-over (Sheikh et al., 1997, Cavey and Lecuit, 2009; Cavey et al., 2008; Engl et al., 2014; Wu et al., 2014), we decided to first check for differences in E-Cadherin, F-actin and phosphorylated Myosin II (pMyosin) protein localization between stage X and 3 epithelia, in dividing cells and their neighbors.

Immunofluorescence on transverse sections at stage 3, showed that E-Cadherin in chick epiblast cells was distributed along the entire apico-basolateral extent of non-dividing epithelial cells; F-actin localized also along the apico-basolateral cortex of epithelial cells whereas pMyosin was predominantly enriched apically (Figures 4A-A"', see also Figure S4 for quantifications of fluorescence intensity profile). Whole mount stainings on fixed embryos showed that, as observed in 4D live imaging experiments, when cells enter division a long E-Cadherin positive cell interface between seemingly distant neighbors (as observed apically) can already be seen basally (Figures 4C-F, white arrowheads, see also Figure S3A-L, n=11 out of 11 cells, 3 embryos). In contrast, examination at stage X, when cell division does not promote epithelial cell intercalation, revealed interesting differences. Whereas E-Cadherin was also found along the whole basolateral extent of epithelial cells, pMyosin and F-actin showed greater accumulation along the basolateral cortex of epithelial cells (Figures 4B-B"', white arrowheads, see also Figure S4 for quantifications of fluorescence intensity profile). Whole mount stainings on fixed specimens showed that as cells enter division, neighboring cells in contact with the dividing cell exhibited a dramatic accumulation of actin and myosin specifically at the basolateral side (Figures 4G-J, white arrows, see also Figures S3M-X, n=9 out of 10 cells, 3 embryos). This accumulation of actin and myosin in neighbors seemed to prevent the formation of a stable basolateral contact between distant neighbors (as observed in stage 3 embryos) since contact-free cell interfaces (devoid of E-Cadherin staining) could be concomitantly observed, right beneath the dividing cells (white arrows and asterisks, Figures 4H-J, see also Figures S3M-X). Such observations are reminiscent of the mechanisms observed in epithelial cells of the *Drosophila* notum (Founounou et al., 2013; Herszterg et al., 2013a), and adhesion disengagement in the *Drosophila* embryo (Guillot and Lecuit, 2013b) during the generation of a daughter-daughter cell interface, although in chick Myosin accumulation and adhesion disengagement of the dividing cell with its neighbor does not take place apically but basolaterally.

We furthermore checked whether differences in actomyosin dynamics between these two stages might underlie cell division mediated rearrangements. We used Fluorescence Recovery After Photo-bleaching (FRAP) to quantitatively measure Myosin II dynamics at the cortex of epithelial cells at stage 3, when cells exhibit cell division mediated rearrangements, and at stage X, when cells do not undergo cell division mediated intercalations and checked for notable differences. To this end, we electroporated a GFP protein fused to the chicken Myosin Light Chain 2 protein (GFP-Myosin), which localized predominantly to the cell cortex and to the actomyosin ring, as cells divided (Figure 4K, left panel). GFP-myosin did not interfere with cell division nor normal embryonic development after 24h (data not shown), strongly arguing that the GFP-Myosin fusion protein does not interfere with endogenous myosin and that it can be used to monitor its dynamics. By performing FRAP on cortical GFP-Myosin of randomly chosen non-dividing cells (figure 4K, right panel), we found that GFP-Myosin dynamics were different between stage X and stage 3. At stage X, when cells do not undergo cell division mediated intercalations, the mobile fraction was much lower (43%, n= 30) than in epithelial cells of stage 3 embryos (62% n=61) (Figure 4L). Thus, these results show that Myosin stability at the cortex is significantly lower in epithelial cells of stage 3 embryos compared to stage X. Altogether these results show that differences in cortical actin and pMyosin localized accumulation and at least in myosin dynamics underlie cell division mediated rearrangements.

Increasing F-actin and myosin stability impairs cell division mediated rearrangements

We finally functionally tested whether such observed differences in actomyosin cytoskeleton between stage X and 3 might regulate cell division mediated intercalations. To this end we took advantage of two compounds: the F-actin stabilizing peptide Jasplakinolide (Bubb et al., 1994), and the MyosinII phosphatase inhibitor Calyculin A (Ishihara et al., 1989) which allowed us to uniformly increase actomyosin stability in all epithelial cells of stage 3 embryos. Both compounds induced F-actin and Myosin enrichment at the cortex of epithelial cells as shown on transverse sections (Figures 5A-A”’ and 5B-B”’, white arrows, see also Figure S4 for quantifications of fluorescence intensity profile) and whole mount embryos (Figures S5A-I). Moreover,

FRAP experiments on GFP-Myosin electroporated embryos at stage 3 showed that in presence of Jasplakinolide and Calyculin A, the mobile fraction was much lower (0.49, n=16 and 0.47, n=11, respectively) than in stage 3 control embryos (Figure 5C). These results confirmed that in these drug treated embryos, myosin stability at the cortex was dramatically increased, resembling dynamics observed in stage X embryos. Notably, we noted an increased colocalization of F-actin with E-Cadherin at cell junctions, in agreement with higher junction stability (Figure S6). We next examined the localization of these proteins in dividing cells and their immediate neighbors (Figure 5D-K). We found that as cells divided in embryos treated with Calyculin A or Jasplakinolide, a dramatic accumulation of pMyosin and F-actin in neighbors was found along the basolateral extent of neighbors, right beneath the dividing cells (Figures 5E-G and 5I-K, white arrows, n=7/9 cells, 3 embryos and 9/13 cells, 3 embryos for Jasplakinolide and Calyculin A respectively). Moreover, contact-free cell interfaces, devoid of E-Cadherin immunostaining, were observed associated with these cortical accumulations of F-actin and pMyosin (Figure 5E-G and 5I-K, white asterisks). These results show that increasing myosin and F-actin stability in epithelial cells prevents the dividing cell from bringing distant neighbors into contact, a situation strikingly reminiscent of cell divisions in stage X embryos, when rearrangement of daughter cells does not take place.

We thus decided to observe the effect of increasing actomyosin stability on epithelial cell rearrangements using live imaging microscopy. To this end, we live imaged embryos incubated with Calyculin A or Jasplakinolide, which allows uniform perturbation of pMyosin and F-actin turn-over within the epithelial embryo (Figure 6A-D). Notably, at the concentrations we used neither Jasplakinolide nor Calyculin A induced a remarkable decrease in cell division (6% decrease for both Jasplakinolide and Calyculin A compared to control embryos, as counted per number of dividing cells/μm^2 per hour, n= 1100 cells analyzed, 4 embryos and n=1111 cells, 3 embryos respectively). Additionally, we electroporated RhoA which enables actomyosin cytoskeleton stabilization in a more selective way due to the mosaic overexpression resulting from the electroporation method (Figure 6E-F and Figure S5J-S), therefore allowing to monitor the behavior of WT dividing cells next to RhoA overexpressing cells (Figure 6E-E”). In both embryos treated with Calyculin A,

Jasplakinolide and in RhoA electroporated embryos, separation of daughter cells was greatly affected, with 85% (n= 181, 3 embryos), 69% (n= 129; 3 embryos) and 80% (n=205, 4 embryos) of daughter cells remaining in contact for at least 30 min after cytokinesis has completed (Figure 6A-F, white arrows, 6K and movie S6), vs. 10% in control memGFP transgenic embryos (n=530; 5 embryos) and 12% in GFP electroporated embryos (n=239, 6 embryos) (Figure 6G-J, and 6K). Moreover, analysis of cell-cell junctions over time revealed that CMI, DCAI and T processes were largely affected in Calyculin A (87% of "stable" junctions; 2% CMI; 4% DCAI and 7% T processes; n=385 junctions analyzed, 3 embryos) and Jasplakinolide (85% "stable" junctions; 3% CMI; 7% DCAI and 5% T processes; n=568 junctions analyzed, 3 embryos) treated embryos (Figure 6L, see also Figure S7). These results show that Calyculin A and Jasplakinolide treatments dramatically increase cell-cell junction stability. Strikingly, the behavior of cell-cell junctions in these conditions resembles the behavior of junctions of a stage X embryo, during which epithelial cells exhibit increased actomyosin levels and cell division does not promote cell rearrangements. Altogether these results show that increasing actomyosin cytoskeleton stability dramatically increases junctional stability over time and prevents dividing cells from remodeling nearby junctions, consequently impairing cell division mediated rearrangements.

Discussion

This study has identified that epithelial rearrangements mediated by cell division underlie the spatial patterning of gastrulation movements in chick. As cells divide and dramatically change shape throughout the epithelial embryo, they bring originally distant cells (their immediate neighbors) into contact, thereby promoting intercalation events. The interplay between the actomyosin of dividing cells and the actomyosin of neighboring non-dividing cells prevents rearrangements at stage X before the onset of gastrulation movements, whereas it favors cell division mediated rearrangements, as gastrulation movements take place. Because cells continuously (although asynchronously) divide within the epithelial embryo, cells constantly rearrange, allowing the generation of properly patterned gastrulation movements (Figure 7).

Cell division as an epithelial cell rearrangement driver

As mentioned above, a direct role for cell division in promoting epithelial cell rearrangements has not been reported to date in *Drosophila, C.elegans, Danio rerio and Xenopus* models. Indeed it has been implied that the generation of a common cell-cell interface between daughter cells might be a conserved feature between Metazoan (Gibson et al., 2006). Luminal mitosis has been observed to be associated with cell dispersal in the mouse ureteric bud (Packard et al., 2013), and more recently, cell division has been observed to be associated with rearrangements during mouse limb ectoderm morphogenesis (Lau et al., 2015), challenging the view that daughter cells do not rearrange upon division. While these studies did not examine the role of cell division in cell-cell intercalation and its effect on epithelial morphogenesis, our findings showing that cell division is required for the generation of gastrulation movements leads us to propose that the formation of new cell-cell contacts following cell division might be a broad regulatory mechanism in epithelium morphogenesis. The observations that cell division appears to be associated with epithelial cell rearrangements in other amniote epithelia is intriguing and shows that special attention should be given to the role of cell division in promoting cell rearrangements, as it is very likely that cell division mediated intercalations in general might underlie various morphogenetic processes in a number of different epithelial tissues in developmental, homeostatic or pathological contexts.

Role of cell division mediated rearrangements in the generation of gastrulation movements

Previous studies have shown that a combination of cell shape changes, mediolateral intercalation and ingression events at the posterior marginal zone of the early embryo drive primitive streak formation and elongation (Rozbicki et al., 2015; Voiculescu et al., 2007, 2014). Such cell interactions have been proposed to be the driving force of gastrulation movements and that the rotational movements would ensue as a "propagation" of the cell displacements taking place at the site of primitive streak formation. However whether specific cell behaviors take place in the epithelial embryo to ensure proper patterning of gastrulation movements had remained unaddressed. In the present study, we focused on such specific cellular behaviors. Our data show

that cell divisions and associated cell rearrangements are required for the proper spatial patterning of gastrulation movements but that they do not drive the movement itself. When cell division mediated rearrangements are inhibited (Aphidicolin and Aminopterin treatments), cell movements can still be observed but the spatial pattern is changed: cells do not display the two symmetrical whorls but instead converge directly towards the primitive streak. An attractive hypothesis is that cell division, through constant cell rearrangements, allows epithelial cells to accommodate (through constant and isotropic stress relaxation) the forces generated by cell-cell interactions taking place at the primitive streak (Rozbicki et al., 2015; Voiculescu et al., 2007, 2014); whereas in absence of cell division the whole epithelial sheet, being greatly stabilized, appears to be consequently pulled towards the primitive streak "as a whole" by these same forces (Figure7); although this remains to be experimentally demonstrated. Interestingly, orientation of cell division is not aligned with tissue flow and UV-laser isolation of epithelial regions shows that daughter cell separation appears to be independent of the local directed strains arising from the primitive streak forming region. Therefore the effect of cell division on global tissue flow cannot solely be explained by a tension-induced stress-relieving mechanism. It is however possible that cell division by promoting constant rearrangements might act by modulating the mechanical properties of the epithelial tissue (e.g. fluidization of the tissue). In the future, it will be particularly interesting to test whether a combination of changes in mechanical properties of the epiblast and local directed strains induced by the primitive streak-forming region could explain large scale tissue movements observed during gastrulation.

Molecular mechanisms underlying cell division mediated rearrangements

We also investigated how cell division mediated intercalations are controlled at the molecular level. We find, similar to what has been described in several *Drosophila* epithelia, that cell division in the early chick epiblast can be regarded as a multicellular process in which immediate neighbors at stage X play a role in the formation of daughter-daughter cell junction; however, as gastrulation movements take place in chick, cell division leads to an opposite outcome (i.e. cell intercalation, Figure 7). We identified two specific behaviors:

intercalation of neighboring cells between daughter cells (CMI) and intercalation of daughter cells between neighbors (DCAI) which consequently lead to dramatic rearrangements in the vicinity of a dividing cell. Interestingly, although CMI implies the addition of a novel junction through cytokinesis, it is somehow similar to T1 and rosette processes described in *Drosophila* (Bertet et al., 2004; Blankenship et al., 2006) as a myosin based contraction (cytokinetic ring in CMI and planar junction shortening in T1/rosette processes) brings in contact originally distant cells. However, we show that in chick, intercalation initiates basally, expands apically and eventually occurs in the plane of the epithelium. It has been shown in other systems that Cadherin engagement triggers contact stabilization and expansion through activation of the Rac1 and Arp2/3 complex (Betson et al., 2002; Nakagawa et al., 2001; Noren et al., 2001; Perez et al., 2008; Verma et al., 2004; Yamada and Nelson, 2007; Yamazaki et al., 2007). These data, together with our results, are in support of basal engagement of E-Cadherin between originally distant neighbors as a critical step in the formation of a stable novel junction and thereby in cell intercalation events. In turn, the mechanisms underlying DCAI are less clear as no specific myosin enrichments could be observed in neighbors (data not shown) that could explain active intercalation of daughter cells, as observed in T1 processes in *Drosophila*. It is possible that DCAI might be a passive consequence of cell division, in a local environment that is permissive to rearrangements or an active process in which daughter cells transiently acquire an "intra-epithelial" motility.

At the molecular level, comparison between stage X and 3 embryos pointed at the actomyosin cytoskeleton in non-dividing cells as a regulator of these behaviors. Strikingly, in stage X embryos when cell division does not drive rearrangements, actin and myosin accumulate basolaterally in immediate neighbors of a dividing cell, formation of a novel contact (between distant neighbors) does not take place and adhesion disengagement between the dividing cells and its neighbors can even be observed. A similar phenomenon has been observed in the *Drosophila* embryo and pupal notum during the formation of daughter-daughter cell interface (Founounou et al., 2013; Guillot and Lecuit, 2013b; Herszterg et al., 2013b), although in chick actomyosin accumulation and adhesion disengagement occur along the basolateral interface. From our analysis, the major difference between the embryonic and pupal notum epithelia in *Drosophila* and the early chick

embryonic epithelium is that E-Cadherin can be found basolaterally in chick epithelial cells. It is thus possible that since myosin and actin do not accumulate basolaterally in epithelial cells of stage 3 embryos, as a dividing cell rounds up, contracts and splits, it can freely deform and displace its immediate and adherent neighbors, bringing them into contact without resistance. We finally demonstrate the functional relevance of actin and myosin in this process by increasing cortical actomyosin accumulation uniformly in the epiblast using Jasplakinolide and Calyculin A, or specifically in neighboring cells using RhoA. Such accumulation of actomyosin at the cortex impairs the formation of novel contacts basally and subsequent cell division mediated rearrangements normally taking place at stage 3, recapitulating situations and behaviors observed at stage X. Taken together our results provide a mechanistical framework for understanding how cell division can lead to different remodeling outcomes within an epithelial tissue and how it impacts its morphogenesis at a mesoscopic scale.

Experimental Procedures

Embryo culture, imaging and laser dissection

Fertilized chicken eggs were ordered from commercial source (EARL Morizeau) and memGFP transgenic chicken eggs were generously provided by Dr. Feifei Song, Dr Adrian Sherman and Dr. Helen Sang (from the Roslin Institute in Edinburgh, Scotland). Eggs were collected at stage X and cultured using a modified version of the EC culture system (Chapman et al., 2001) until stage 3^+ and transferred into bottom glass Petri dish (Mattek inc.) with semi solid albumen/agarose (0.2%) for imaging, with or without drugs: Aphidicolin (30-50μM), Aminopterin (100μM), Jasplakinolide (10μM) and Calyculin A (0.1μM). Embryos were then imaged at 38 degrees using an inverted confocal microscope (Zeiss LSM 700 and LSM880) or a 2-photon Microscope (Zeiss, NLO LSM 7MP) coupled to a Chameleon Ti/Saph laser (Coherent inc.) at 840nm wavelength using 10x, 40X or 63X long distance objectives. The tiling/stitching feature of the Zen software (Zeiss) was used to acquire large embryonic regions (about $1mm^2$/5000-10000 cells) with a 40x objective. Laser microdissections were performed using a 355nm pulsed laser (35%-50% power), a UGA-42 module from Rapp Optoelectronic coupled to a Zeiss LSM 880 and a 10x objective.

Image analysis and quantifications

Images were analyzed using ImageJ and Imaris (Bitplane) softwares. All quantifications were performed manually on registrated movies (Thévenaz et al., 1998) by visual inspection, following cells or junctions across time. For all experiments, daughter cells were scored as separated when they did not share a common interface 30min after the completion of cytokinesis. Quantifications of daughter cell separation at stage X were performed during the first 3 hours of development and within 3 hours after exposure to the drugs in stage 3 embryos. For cell-cell junction analysis, 1 hour-long movies were analyzed; regions were randomly chosen but the number of cell division per total number of junctions analyzed within these regions was kept constant, except for Aphidicolin and Aminopterin treated embryos in which cell division was largely inhibited. Junctions were classified into four different states, based on whether the cell-cell junction exhibited

neighbor exchange: Stable: pair of neighbors remained unchanged; T transition: T1 or T2 process (i.e. cell division-independent neighbor exchange); CMI transition: dividing cell-neighbor junction involved in an intercalation event between daughter cells; DCAI transition: T1 process involving a daughter cell (see Movie S3. The rate of cell division in drug treated embryos were measured by counting the number of dividing cell per mm^2 and per hour normalized to stage 3 embryos rates.

FRAP experiments

For FRAP experiments, embryos were electroporated with GFP-Myosin at stage X and then incubated for 5h until clear cortical GFP-Myosin signal could be visualized. For stage 3, the same embryos where FRAP was performed at stage X were kept incubated overnight for a total incubation time of 14h. The GFP-Myosin signal did not show any significant difference in intensity between both stages and identical photobleaching and imaging conditions were used. A 10x10 pixels cortical region was photobleached using a 488nm laser at 100% (pixel dwell time of 100 µs for 10 iterations). Cells were then imaged every 1.5s for at least 250s using a Zeiss LSM700 confocal and a 40x objective. All quantifications were performed in Fiji. Images were adjusted for xy drift with the plugin: "Linear Stack Alignment with SIFT" using a translational transformation. ROIs within the bleached and within non-bleached areas were then manually selected in order to compensate for acquisition bleach and to normalize the values. The curve fitting of the data was done using a custom made plugin in Matlab (MathWorks). Final plots were done using Prism (GraphPad Software).

Chick Embryo Electroporation and Immunofluorescence

Embryos were electroporated with RhoA/GFP (kind gift from Gojun Sheng) or GFP only, in custom made electroporation chambers using a NEPA21 (Sonidel) electroporator with 2 poring pulses of 15V, 5ms delay, and 3 transfer pulses of 10V, 50ms delay. Electroporated embryos were incubated with Cell Mask Deep Red (Invitrogen) prior to live imaging experiments. Briefly, 0.5µl of Cell Mask Deep Red stock solution ($5mg.ml^{-1}$ in DMSO) was diluted in 250µl of HBSS; 50ul of this dilution was then deposited on the ventral

side of the embryo and incubated for 15min prior to imaging. For antibody stainings, embryos were incubated with Phalloidin- Alexa 488 (1/100, Molecular Probes), antibodies against E-Cadherin (1/500, BD science), pMyosinII (1/50, Cell signaling), and Hoechst (1/1000, Molecular Probes) overnight, washed 24h, incubated overnight with Alexa-coupled secondary antibodies and washed 24h. All incubation and washes were performed in (PBS/BSA 0.2%, Triton 0,1% / SDS 0,02%). Embryos were then mounted between slide and coverslip and imaged using a Zeiss LSM700 or LSM880.

Author contribution

J.G. conceived the project and designed experiments, J.F. and D.R. conducted most experiments with help from J.G. and M.S. on large scale live imaging and analysis, C.M. helped with various quantifications of cell behavior and image analysis, J.G. wrote the paper with comments from co-authors.

Acknowledgements

We thank F. Schweisguth for insightful discussions; M. Yanniv, S. Tajbakhsh, F. Schweisguth, S. Hopyan, C. Tabin and T. Lecuit for critical reading of the manuscript; H. Sang, F. Song and A. Sherman for sharing the memGFP transgenic chicken eggs prior publication (from the transgenic chicken facility of the Roslin Institute in Edinburgh, Scotland, supported by the Wellcome Trust) and J.Y. Tinevez for help with the FRAP analysis. Research in J. Gros laboratory is funded by the Institut Pasteur, the CNRS, the Vallee Foundation Young Investigator Award, the Cercle FSER, a starting grant from the FRM, and ERC starting Grant.

References

Baena-López, L.A., Baonza, A., and García-Bellido, A. (2005). The orientation of cell divisions determines the shape of Drosophila organs. Curr. Biol. *15*, 1640–1644.

Bertet, C., Sulak, L., and Lecuit, T. (2004). Myosin-dependent junction remodelling controls planar cell intercalation and axis elongation. Nature *429*, 667–671.

Betson, M., Lozano, E., Zhang, J., and Braga, V.M.M. (2002). Rac activation upon cell-cell contact formation is dependent on signaling from the epidermal growth factor receptor. J. Biol. Chem. *277*, 36962–36969.

Bischoff, M., and Cseresnyés, Z. (2009). Cell rearrangements, cell divisions and cell death in a migrating epithelial sheet in the abdomen of Drosophila. Development (Cambridge, England) *136*, 2403–2411.

Blankenship, J.T., Backovic, S.T., Sanny, J.S.P., Weitz, O., and Zallen, J.A. (2006). Multicellular rosette formation links planar cell polarity to tissue morphogenesis. Dev. Cell *11*, 459–470.

Bubb, M.R., Senderowicz, A.M., Sausville, E.A., Duncan, K.L., and Korn, E.D. (1994). Jasplakinolide, a cytotoxic natural product, induces actin polymerization and competitively inhibits the binding of phalloidin to F-actin. J. Biol. Chem. *269*, 14869–14871.

Campinho, P., Behrndt, M., Ranft, J., Risler, T., Minc, N., and Heisenberg, C.-P. (2013). Tension-oriented cell divisions limit anisotropic tissue tension in epithelial spreading during zebrafish epiboly. Nature Cell Biology *15*, 1405–1414.

Cavey, M., and Lecuit, T. (2009). Molecular Bases of Cell–Cell Junctions Stability and Dynamics. Cold Spring Harb Perspect Biol *1*, a002998.

Cavey, M., Rauzi, M., Lenne, P.-F., and Lecuit, T. (2008). A two-tiered mechanism for stabilization and immobilization of E-cadherin. Nature *453*, 751–756.

Chapman, S.C., Collignon, J., Schoenwolf, G.C., and Lumsden, A. (2001). Improved method for chick whole-embryo culture using a filter paper carrier. Dev. Dyn. *220*, 284–289.

Concha, M.L., and Adams, R.J. (1998). Oriented cell divisions and cellular morphogenesis in the zebrafish gastrula and neurula: a time-lapse analysis. Development *125*, 983–994.

Cui, C., Yang, X., Chuai, M., Glazier, J. a, and Weijer, C.J. (2005). Analysis of tissue flow patterns during primitive streak formation in the chick embryo. Developmental Biology *284*, 37–47.

Engl, W., Arasi, B., Yap, L.L., Thiery, J.P., and Viasnoff, V. (2014). Actin dynamics modulate mechanosensitive immobilization of E-cadherin at adherens junctions. Nat Cell Biol *16*, 587–594.

Founounou, N., Loyer, N., and Le Borgne, R. (2013). Septins regulate the contractility of the actomyosin ring to enable adherens junction remodeling during cytokinesis of epithelial cells. Dev. Cell *24*, 242–255.

Gibson, M.C., Patel, A.B., Nagpal, R., and Perrimon, N. (2006). The emergence of geometric order in proliferating metazoan epithelia. Nature *442*, 1038–1041.

Gong, Y., Mo, C., and Fraser, S.E. (2004). Planar cell polarity signalling controls cell division orientation during zebrafish gastrulation. Nature *430*, 689–693.

Gräper, L. (1929). Die Primitiventwicklung des Hühnchens nach stereokinematographischen Untersuchungen, kontrolliert durch vitale Farbmarkierung und verglichen mit der Entwicklung anderer Wirbeltiere. Development Genes and Evolution *116*, 382–429.

Guillot, C., and Lecuit, T. (2013a). Mechanics of epithelial tissue homeostasis and morphogenesis. Science (New York, N.Y.) *340*, 1185–1189.

Guillot, C., and Lecuit, T. (2013b). Adhesion disengagement uncouples intrinsic and extrinsic forces to drive cytokinesis in epithelial tissues. Dev. Cell *24*, 227–241.

Harrell, J.R., and Goldstein, B. (2011). Internalization of multiple cells during C. elegans gastrulation depends on common cytoskeletal mechanisms but different cell polarity and cell fate regulators. Developmental Biology *350*, 1–12.

Herszterg, S., Leibfried, A., Bosveld, F., Martin, C., and Bellaiche, Y. (2013a). Interplay between the dividing cell and its neighbors regulates adherens junction formation during cytokinesis in epithelial tissue. Developmental Cell *24*, 256–270.

Herszterg, S., Leibfried, A., Bosveld, F., Martin, C., and Bellaiche, Y. (2013b). Interplay between the dividing cell and its neighbors regulates adherens junction formation during cytokinesis in epithelial tissue. Dev. Cell *24*, 256–270.

Ishihara, H., Martin, B.L., Brautigan, D.L., Karaki, H., Ozaki, H., Kato, Y., Fusetani, N., Watabe, S., Hashimoto, K., and Uemura, D. (1989). Calyculin A and okadaic acid: inhibitors of protein phosphatase activity. Biochem. Biophys. Res. Commun. *159*, 871–877.

Kieserman, E.K., Glotzer, M., and Wallingford, J.B. (2008). Developmental Regulation of Central Spindle Assembly and Cytokinesis during Vertebrate Embryogenesis. Current Biology *18*, 116–123.

Knox, A.L., and Brown, N.H. (2002). Rap1 GTPase Regulation of Adherens Junction Positioning and Cell Adhesion. Science *295*, 1285–1288.

Lau, K., Tao, H., Liu, H., Wen, J., Sturgeon, K., Sorfazlian, N., Lazic, S., Burrows, J.T.A., Wong, M.D., Li, D., et al. (2015). Anisotropic stress orients remodelling of mammalian limb bud ectoderm. Nat. Cell Biol. *17*, 569–579.

LeGoff, L., Rouault, H., and Lecuit, T. (2013). A global pattern of mechanical stress polarizes cell divisions and cell shape in the growing Drosophila wing disc. Development *140*, 4051–4059.

Mao, Y., Tournier, A.L., Hoppe, A., Kester, L., Thompson, B.J., and Tapon, N. (2013). Differential proliferation rates generate patterns of mechanical tension that orient tissue growth. EMBO J. *32*, 2790–2803.

Marinari, E., Mehonic, A., Curran, S., Gale, J., Duke, T., and Baum, B. (2012). Live-cell delamination counterbalances epithelial growth to limit tissue overcrowding. Nature *484*, 542–545.

Morin, X., and Bellaïche, Y. (2011). Mitotic spindle orientation in asymmetric and symmetric cell divisions during animal development. Dev. Cell *21*, 102–119.

Nakagawa, M., Fukata, M., Yamaga, M., Itoh, N., and Kaibuchi, K. (2001). Recruitment and activation of Rac1 by the formation of E-cadherin-mediated cell-cell adhesion sites. J. Cell. Sci. *114*, 1829–1838.

Noren, N.K., Niessen, C.M., Gumbiner, B.M., and Burridge, K. (2001). Cadherin engagement regulates Rho family GTPases. J. Biol. Chem. *276*, 33305–33308.

Olivier, N., Luengo-Oroz, M.A., Duloquin, L., Faure, E., Savy, T., Veilleux, I., Solinas, X., Débarre, D., Bourgine, P., Santos, A., et al. (2010). Cell lineage reconstruction of early zebrafish embryos using label-free nonlinear microscopy. Science *329*, 967–971.

Packard, A., Georgas, K., Michos, O., Riccio, P., Cebrian, C., Combes, A.N., Ju, A., Ferrer-Vaquer, A., Hadjantonakis, A.-K., Zong, H., et al. (2013). Luminal mitosis drives epithelial cell dispersal within the branching ureteric bud. Developmental Cell *27*, 319–330.

Perez, T.D., Tamada, M., Sheetz, M.P., and Nelson, W.J. (2008). Immediate-Early Signaling Induced by E-cadherin Engagement and Adhesion. J. Biol. Chem. *283*, 5014–5022.

Rozbicki, E., Chuai, M., Karjalainen, A.I., Song, F., Sang, H.M., Martin, R., Knölker, H.-J., MacDonald, M.P., and Weijer, C.J. (2015). Myosin-II-mediated cell shape changes and cell intercalation contribute to primitive streak formation. Nat Cell Biol *17*, 397–408.

Saburi, S., Hester, I., Fischer, E., Pontoglio, M., Eremina, V., Gessler, M., Quaggin, S.E., Harrison, R., Mount, R., and McNeill, H. (2008). Loss of Fat4 disrupts PCP signaling and oriented cell division and leads to cystic kidney disease. Nat. Genet. *40*, 1010–1015.

Sheikh, S., Gratzer, W.B., Pinder, J.C., and Nash, G.B. (1997). Actin polymerisation regulates integrin-mediated adhesion as well as rigidity of neutrophils. Biochem. Biophys. Res. Commun. *238*, 910–915.

da Silva, S.M., and Vincent, J.-P. (2007). Oriented cell divisions in the extending germband of Drosophila. Development *134*, 3049–3054.

Thévenaz, P., Ruttimann, U.E., and Unser, M. (1998). A pyramid approach to subpixel registration based on intensity. IEEE Transactions on Image Processing : A Publication of the IEEE Signal Processing Society *7*, 27–41.

Truong Quang, B.-A., Mani, M., Markova, O., Lecuit, T., and Lenne, P.-F. (2013). Principles of E-Cadherin Supramolecular Organization In Vivo. Current Biology *23*, 2197–2207.

Verma, S., Shewan, A.M., Scott, J.A., Helwani, F.M., den Elzen, N.R., Miki, H., Takenawa, T., and Yap, A.S. (2004). Arp2/3 activity is necessary for efficient formation of E-cadherin adhesive contacts. J. Biol. Chem. *279*, 34062–34070.

Voiculescu, O., Bertocchini, F., Wolpert, L., Keller, R.E., and Stern, C.D. (2007). The amniote primitive streak is defined by epithelial cell intercalation before gastrulation. Nature *449*, 1049–1052.

Voiculescu, O., Bodenstein, L., Lau, I.-J., and Stern, C.D. (2014). Local cell interactions and self-amplifying individual cell ingression drive amniote gastrulation. eLife Sciences *3*, e01817.

Wetzel, R. (1929). Untersuchungen am Hühnchen. Die Entwicklung des Keims während der ersten beiden Bruttage. W. Roux' Archiv f. Entwicklungsmechanik *119*, 188–321.

Wu, S.K., Gomez, G.A., Michael, M., Verma, S., Cox, H.L., Lefevre, J.G., Parton, R.G., Hamilton, N.A., Neufeld, Z., and Yap, A.S. (2014). Cortical F-actin stabilization generates apical–lateral patterns of junctional contractility that integrate cells into epithelia. Nature Cell Biology *16*, 167–178.

Wyatt, T.P.J., Harris, A.R., Lam, M., Cheng, Q., Bellis, J., Dimitracopoulos, A., Kabla, A.J., Charras, G.T., and Baum, B. (2015). Emergence of homeostatic epithelial packing and stress dissipation through divisions oriented along the long cell axis. PNAS *112*, 5726–5731.

Yamada, S., and Nelson, W.J. (2007). Localized zones of Rho and Rac activities drive initiation and expansion of epithelial cell-cell adhesion. J. Cell Biol. *178*, 517–527.

Yamazaki, D., Oikawa, T., and Takenawa, T. (2007). Rac-WAVE-mediated actin reorganization is required for organization and maintenance of cell-cell adhesion. J. Cell. Sci. *120*, 86–100.

Figure Legends

Figure 1. Cell division drives epithelial cell intercalation.

(A) Maximum projection of time series from a 3-hour time-lapse experiment of a chick embryo electroporated with a GFP reporter gene, showing the counter rotational movements of epiblast cells at stage 3+, the primitive streak is indicated by a red dotted line.

(B) Time series in a region away from the primitive streak equivalent to the boxed region in (A) showing that upon cell division, daughter cells (white arrow) separate away from each other (red arrow).

(C) Dorsal view of a stage3 memGFP transgenic chicken embryo acquired with a 10x and the tiling/stitching module of the confocal microscope. The dotted white boxes depict the regions analyzed in (D)

(D) Percentage of daughter cell separation following cell division between stage X and 3+. Cell separation was scored every 2 hours, n=2997, 7 embryos.

(E and **F)** Time series of a stage X (E) and stage 3 (F) memGFP transgenic chick embryo highlighting the fate of a dividing cell (in red) and its immediate neighbors (in blue). At stage X (E) daughter cells do not rearrange.

(G) Image of a memGFP transgenic chick embryo from a time-lapse experiment highlighting daughter cells (colored cells) that have rearranged within 30min after cell division.

Scale bar is 200μm in (A), 500μm in (C) and 10μm in (B and E-F). See also Movies S1 and S2.

Figure 2. Cell division events and their associated rearrangements are necessary for the spatial patterning of gastrulation movements.

(A-C) Maximum projection of time series from a time-lapse experiment of a WT GFP electroporated embryo. The last ten time points have been pseudo-colored in red, the position of the primitive streak is indicated by a red dotted line. (A'-C') Cartoon depicting the trajectories of a few cells.

(D) First time point of a 1hour time-lapse experiment of a memGFP WT embryo, showing the region used for junction transition analyses in (D'). (D') Cartoon schematizing transitions that each cell-cell junction will undergo over 1h in the region boxed in (D). "Stable" junctions, CMI and DCAI "T" transitions are shown in grey, light blue, dark blue and orange, respectively (see experimental procedure and movie S3, for explanation on junction state assignment) ; cells that will divide are colored in red.

(E) Time series of a WT memGFP embryo on which stripes of cells and their progeny have been artificially labelled (in blue, green and red) to reveal changes in cell organization between (t0) (E) and t+100min (E'). Note that in WT embryos cells disperse widely.

(F) Quantifications of the relative proportion of Stable, CMI, DCAI and T processes transitions in WT, Aphidicolin and Aminopterin treated embryos.

(G-I) Maximum projection of time series from a time-lapse experiment of an Aphidicolin treated and GFP electroporated embryo. (G'-I') Cartoon depicting the trajectories of a few cells.
(J) First time point of a 1hour time-lapse experiments of a memGFP WT embryo, showing the region used for junction transition analyses in (J'). (J') Cartoon schematizing transitions that each cell-cell junction will undergo over 1h in the region boxed in (J). The same color code used in (D) is applied.
(K) Time series of an Aphidicolin treated memGFP embryo on which stripes of cells and their progeny have been artificially labelled (in blue, green and red) to reveal changes in cell organization between t0 (K) and t+100min (K''). Note that the cellular organization remains almost unchanged. Error bars represent SEM with χ^2 test p-value between bars <0.0001 (****).
Scale bar is 200μm in (A to C, D to F) and 10 μm in (G to J). See also Figure S1, Movies S3 and S4.

Figure 3. Cell division actively promotes epithelial rearrangements
(A) Dorsal view of a stage3 memGFP transgenic chicken embryo acquired with a 10x and the tiling/stitching module of the confocal microscope. The white box depicts the location of regions analyzed, as shown in (B).
(B) Maximum intensity projection of time points of a 1 hour time lapse experiment in a region lateral to the primitive streak as shown in (A). Red lines point at cell divisions which lead to daughter cell juxtaposition, green lines to daughter cells that separate from each other. Projection of the memGFP signal allows the visualization of the global tissue movement.
(C) Quantification of cell division orientation normalized to local tissue movement (red arrow). Note that no specific alignment of cell division with tissue flow can be observed (χ^2 test, p-value= 0.85).
(D) Dorsal view of a stage3 memGFP transgenic chicken embryo acquired with a 10x and the tiling/stitching module of the confocal microscope. The dotted white circle depicts a region that was laser-isolated.
(E) Maximum intensity projection of time points of a 1 hour time lapse experiment of the laser-isolated region shown in (E). Red lines point at cell divisions which lead to daughter cell juxtaposition, green lines daughter cells that separate from each other. Projection of the memGFP signal allow the visualization of the global tissue movement. Note that tissue flow is normal outside of the isolated region but abrogated in the isolated region.
(F) Quantifications of the proportion of daughter cell separation in control and laser-isolated epithelial regions (light grey: separated daughter cells; dark grey: daughter cells in contact). 2 way ANOVA test showed no significant difference (ns).
Scale bar is 500μm in (A and D) and 200 μm in (B) and 100μm in (E). See also Movie S5.

Figure 4. E-Cadherin, F-actin and pMyosin localization and myosin dynamics before and during gastrulation movements.

(A and B) Transverse cryosections of stage 3 (A) and stage X (B) embryos stained with Phalloidin (A and B), pMyosin (A' and B') and E-Cadherin (A" and B") antibodies. (A"' and B"') show the merged pictures.

(C-J) Confocal ortho-slices of stage 3 (C-F) and stage X (G-J) whole mount embryos stained with Phalloidin, pMyosin and E-Cadherin antibodies. Arrows point at F-actin and pMyosin accumulation, asterisks show free-contact cell interfaces, arrowheads point at basal E-Cadherin junctions.

(K) Left panel: time series of a GFP-Myosin electroporated cell showing localization at the cortex and at the cytokinetic furrow in a stage 3 embryo. Right panel: Example of images used for GFP-Myosin (heatmap color code) FRAP experiments, showing the region used for FRAP (arrowhead) of epithelial cells in stage X and 3 embryos.

(L) Left panel: FRAP curves of cortical GFP-Myosin in stage X (red) and stage3 (blue) embryos, errors bars indicate SEM, n= 30 and 61 for stage X and stage 3, respectively. Right panel: Common plot of mobile fraction for all FRAP experiments done at stage X and 3; associated average numbers of the mobile fraction of each fitted curve and statistical significance between the two stages obtained by a Mann Whitney t test, p-value < 10^{-5}(****).

Scale bar is 10μm. See also Figure S2, S3 and S4.

Figure 5. Calyculin A and Jasplakinolide treatment induce basolateral accumulation of myosin in cells neighboring a dividing cell.

(A and B) Transverse cryosections of Calyculin A (A) and Jasplakinolide (B) treated embryos stained with Phalloidin (A and B) pMyosin (A' and B') and E-Cadherin (A" and B') antibodies. (A"' and B"') show the merged pictures.

(C) Left panel: FRAP curves of cortical GFP-Myosin in Jasplakinolide (yellow) and Calyculin A treated embryos, errors bars indicate SEM, n= 16 and 11 for Jasplakinolide and Calyculin A, respectively. Stage X and Stage 3 GFP-Myosin FRAP profiles have been added for reference. Right panel: Common plot of mobile fraction for all FRAP experiments and statistical significance between the different conditions obtained by a Mann Whitney t test; ns, not significant; p-value <0.05 (*).

(D-K) Confocal ortho-slices of Calyculin A (C-F) and Jasplakinolide (G-J) whole mount embryos stained with Phalloidin, pMyosin and E-Cadherin antibodies. Asterisk show contact-free cell interfaces (E-Cadherin free) and white arrows point at pMyosin and F-actin basolateral accumulation.

See also Figure S4 and S5.

Figure 6. Actin and myosin dynamics control cell division mediated intercalation.

(A-D) Time series of a memGFP transgenic embryo treated with: the myosin phosphatase inhibitor Calyculin A (A) or the F-actin stabilizer Jasplakinolide (C) with corresponding Kymograph (B, D) of the region boxed in (A, C) revealing the relationship between daughter cells at every time point of the movie.

(E and F) Time series of a RhoA/GFP electroporated embryo and incubated with the Cell Mask membrane dye (red) with corresponding Kymograph (F) of the region boxed in (E).

(G and H) Time series of memGFP transgenic embryo with corresponding Kymograph (H) of the region boxed in (G).

(I and J) Time series of a GFP electroporated embryo and incubated with the Cell Mask membrane dye (red) with corresponding Kymograph (J) of the region boxed in (I).

(K) Quantification of the proportion of cells exhibiting a daughter-daughter cell junction in all aforementioned conditions. Error bars represent SEM with 2 way ANOVA test p-value between bars <0.0001 (****)**.**

(L) Quantifications of the relative proportion of Stable junctions, CMI, DCAI and T transitions in WT, Calyculin A and Jasplakinolide treated embryos. Error bars represent SEM with χ^2 test p-value between bars <0.0001 (****)**.**

Arrowheads point at a novel junction between initially distant neighbors, arrows point at a daughter-daughter cell junction and red asterisks indicate a dividing cell and its resulting daughter cells. Scale bar is 10μm. See also Figure S5, S6, S7 and Movie S6.

Figure 7. Model for the role and control of cell division during gastrulation.

Higher panel: at stage X, before gastrulation movements initiate epithelial cells divide without promoting rearrangements; epithelial cells exhibit higher actomyosin accumuluation: the dividing cell induces very local deformation of neighbors; as they resist deformation and exhibit high junctional stability (double arrows in blue), these cells consequently fail to move in between daughters and intercalation does not take place.

Middle Panel: at stage 3, as gastrulation movements are taking place, cell division promotes epithelial cell rearrangements; epithelial cells exhibit lower actomyosin accumulation enabling dividing cells to deform and displace neighbors (light blue arrow), bringing them in between the resulting daughters. **Lower panel**: In absence of cell division, epithelial stability is increased as cell division mediated rearrangements do not take

place; epithelial cells are likely pulled (red arrows) towards the primitive streak, where intercalation/ingression events take place (Rozbicki et al., 2015; Voiculescu et al., 2007, 2007).

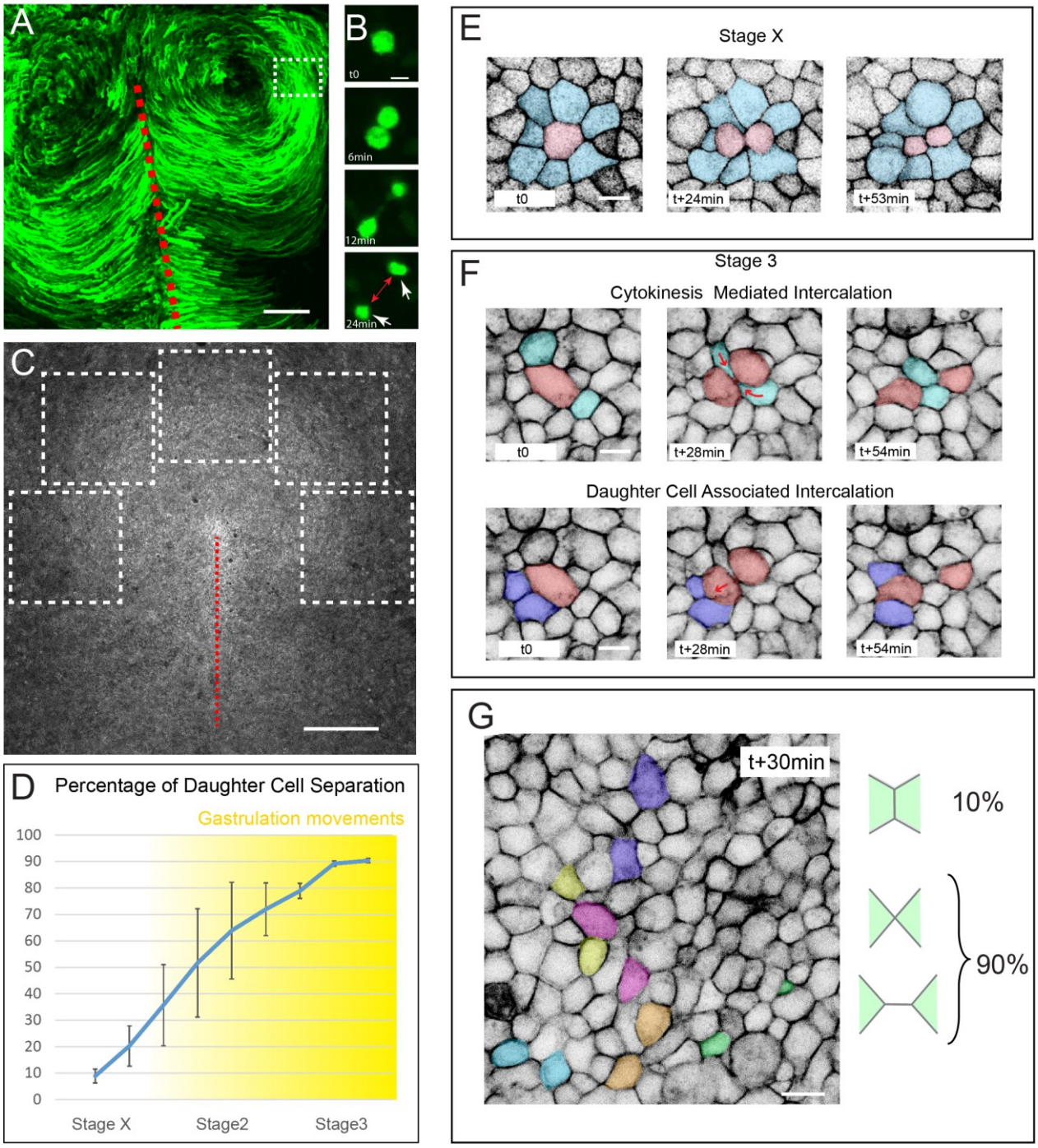
A
B
t0
6min
12min
24min
C
D
Percentage of Daughter Cell Separation
Gastrulation movements
100
90
80
70
60
50
40
30
20
10
0
Stage X
Stage2
Stage3
E
Stage X
t0
t+24min
t+53min
F
Stage 3
Cytokinesis Mediated Intercalation
t0
t+28min
t+54min
Daughter Cell Associated Intercalation
t0
t+28min
t+54min
G
t+30min
10%
90%

Figure 1

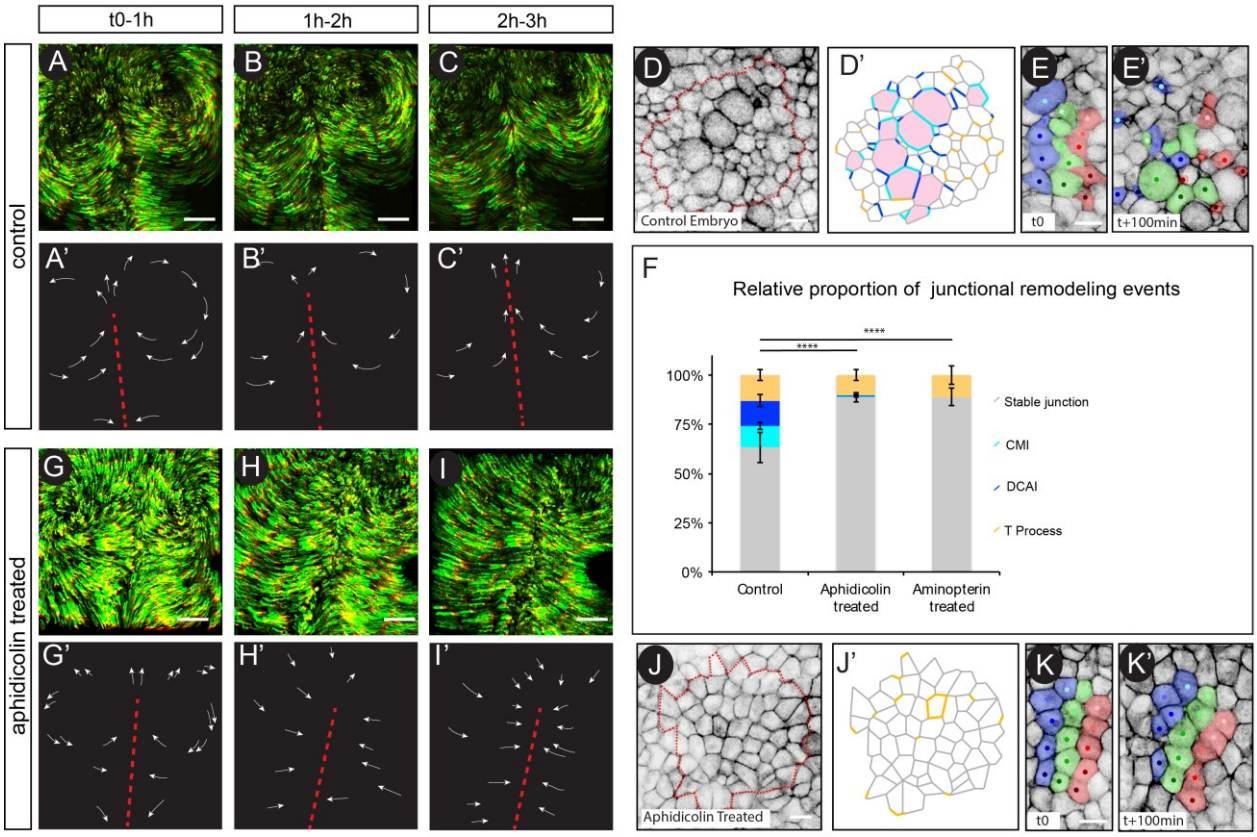
t0-1h
1h-2h
2h-3h
control
aphidicolin treated
A
B
C
A'
B'
C'
G
H
I
G'
H'
I'
D
D'
E
E'
Control Embryo
t0
t+100min
F
Relative proportion of junctional remodeling events
****
****
100%
75%
50%
25%
0%
Control
Aphidicolin treated
Aminopterin treated
Stable junction
CMI
DCAI
T Process
J
J'
K
K'
Aphidicolin Treated
t0
t+100min

Figure 2

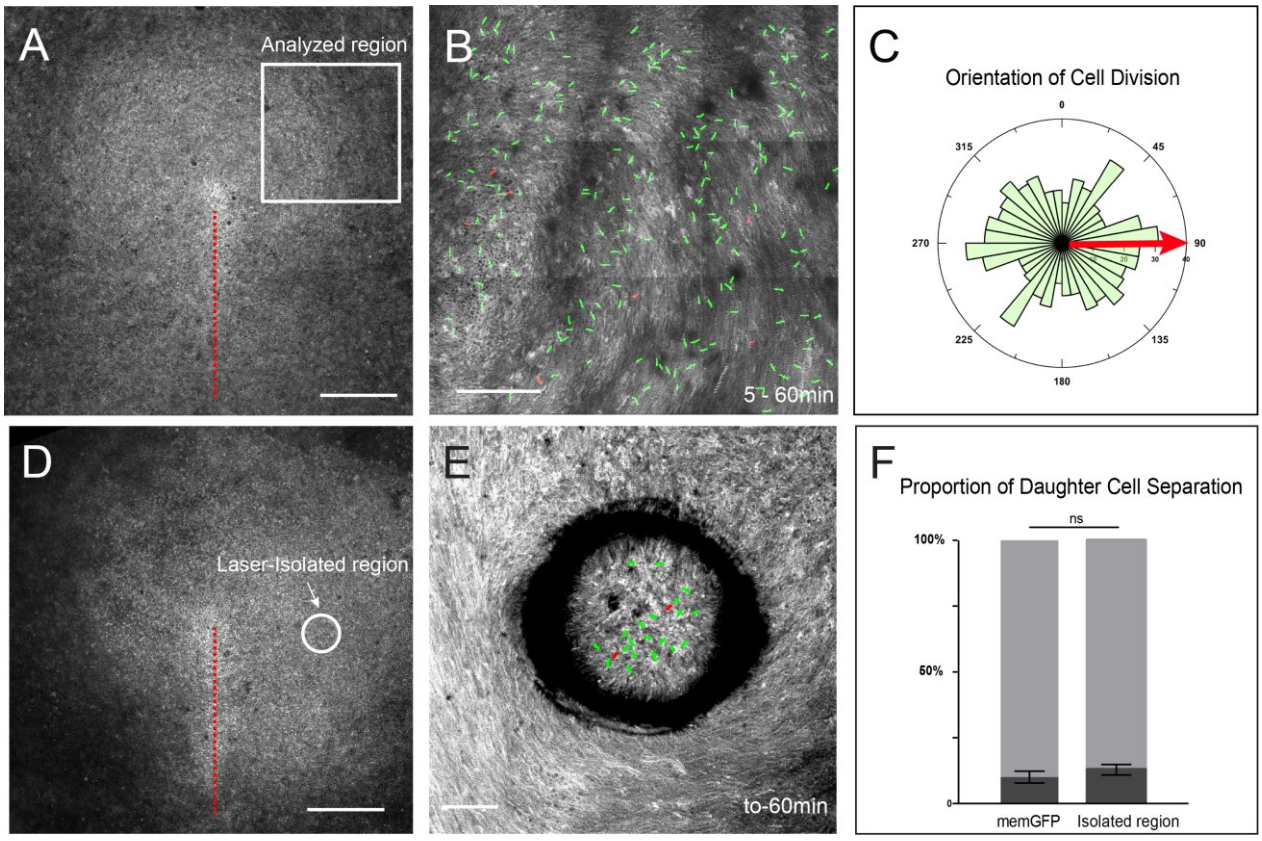
A
Analyzed region
B
5 - 60min
C
Orientation of Cell Division
0
45
90
135
180
225
270
315
D
Laser-Isolated region
E
to-60min
F
Proportion of Daughter Cell Separation
ns
100%
50%
0
memGFP
Isolated region

Figure 3

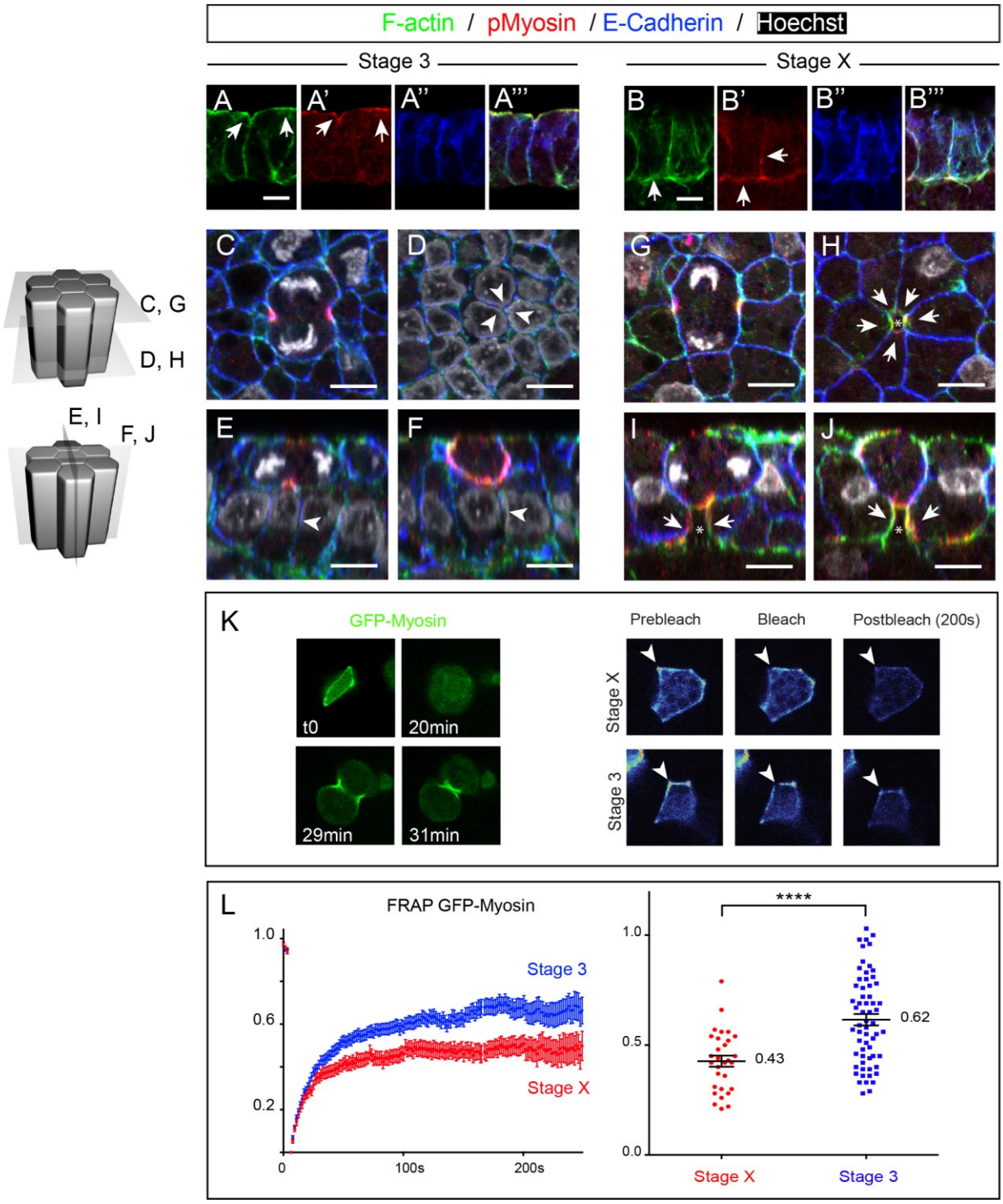
F-actin / pMyosin / E-Cadherin / Hoechst
Stage 3
Stage X
A
A'
A''
A'''
B
B'
B''
B'''
C, G
D, H
E, I
F, J
C
D
E
F
G
H
I
J
K
GFP-Myosin
t0
20min
29min
31min
Prebleach
Bleach
Postbleach (200s)
Stage X
Stage 3
L
FRAP GFP-Myosin
1.0
0.6
0.2
0
100s
200s
Stage 3
Stage X
****
1.0
0.5
0.0
0.43
0.62
Stage X
Stage 3

Figure 4

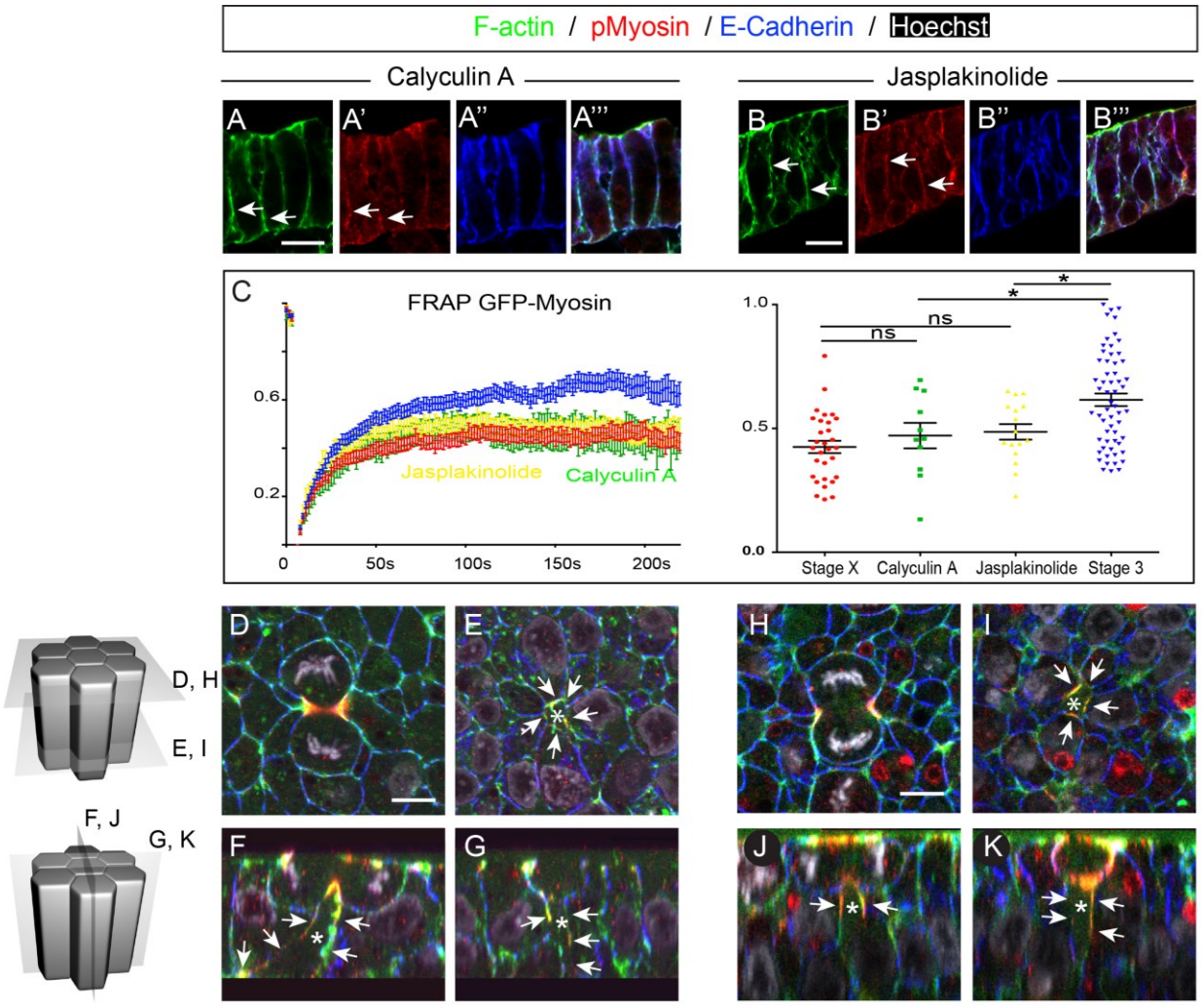
F-actin / pMyosin / E-Cadherin / Hoechst
Calyculin A
Jasplakinolide
A
A'
A''
A'''
B
B'
B''
B'''
C
FRAP GFP-Myosin
0.6
0.2
0
50s
100s
150s
200s
Jasplakinolide
Calyculin A
1.0
0.5
0.0
ns
ns
*
*
Stage X
Calyculin A
Jasplakinolide
Stage 3
D, H
E, I
F, J
G, K
D
E
F
G
H
I
J
K

Figure 5

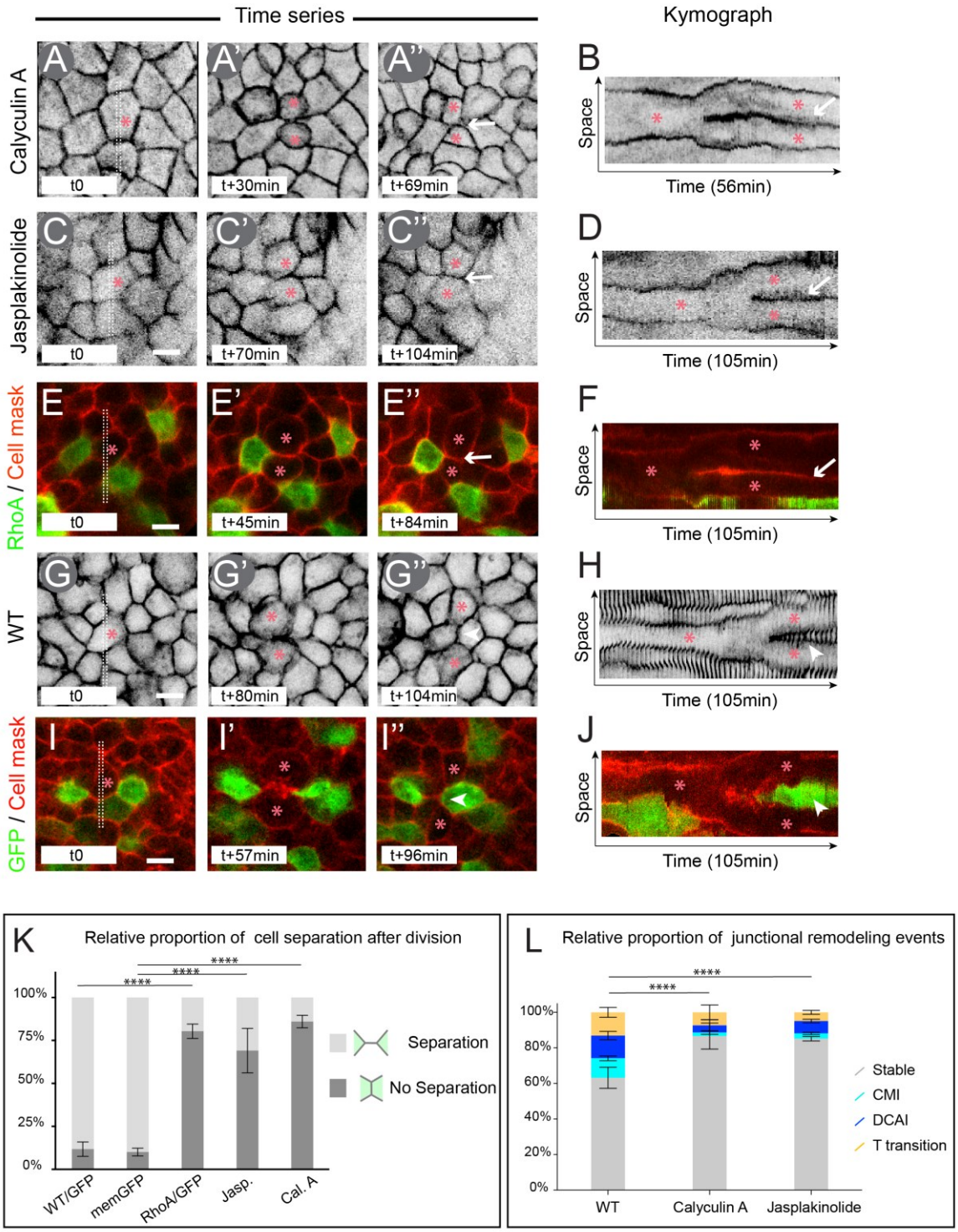
Time series
Kymograph
Calyculin A
Jasplakinolide
RhoA / Cell mask
WT
GFP / Cell mask
A
A'
A''
B
C
C'
C''
D
E
E'
E''
F
G
G'
G''
H
I
I'
I''
J
t0
t+30min
t+69min
t+70min
t+104min
t+45min
t+84min
t+80min
t+57min
t+96min
Space
Time (56min)
Time (105min)
K
Relative proportion of cell separation after division
100%
75%
50%
25%
0%
****
Separation
No Separation
WT/GFP
memGFP
RhoA/GFP
Jasp.
Cal. A
L
Relative proportion of junctional remodeling events
80%
60%
40%
20%
Stable
CMI
DCAI
T transition
WT
Calyculin A
Jasplakinolide

Figure 6

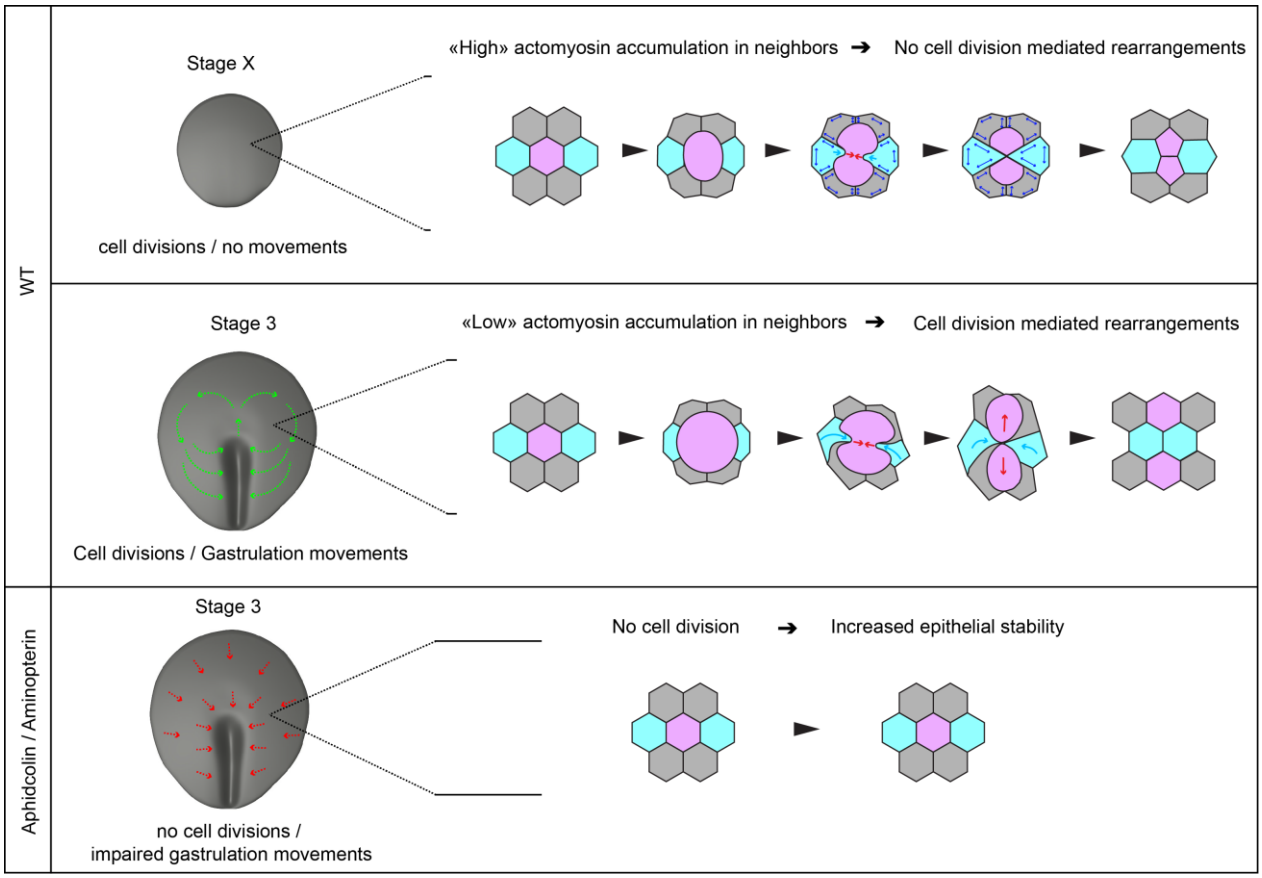
WT
Stage X
«High» actomyosin accumulation in neighbors ➔ No cell division mediated rearrangements
cell divisions / no movements
Stage 3
«Low» actomyosin accumulation in neighbors ➔ Cell division mediated rearrangements
Cell divisions / Gastrulation movements
Aphidcolin / Aminopterin
Stage 3
No cell division ➔ Increased epithelial stability
no cell divisions /
impaired gastrulation movements

Figure 7

Supplemental Figures

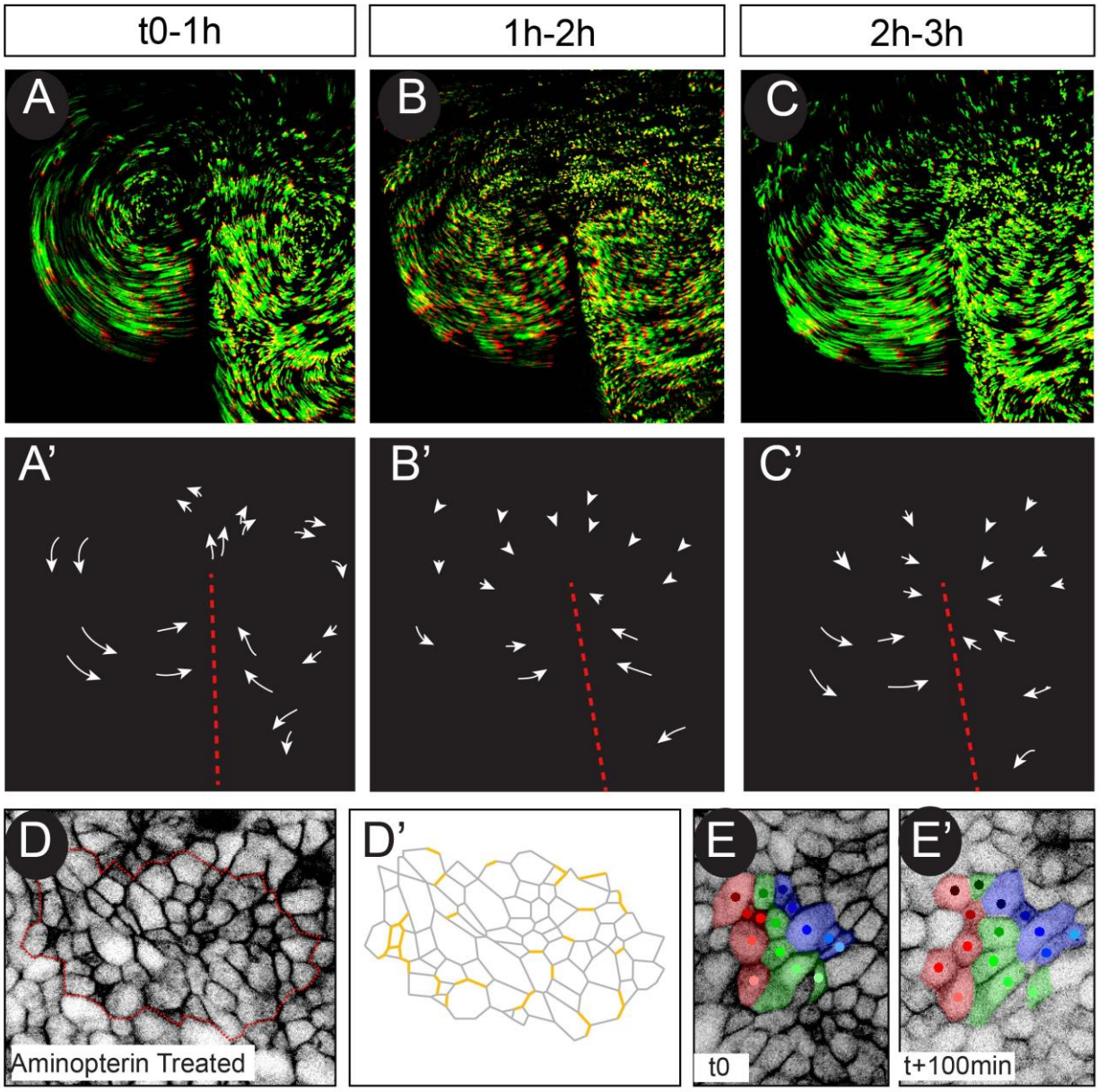

Figure S1, related to Figure 2. The cell division inhibitor Aminopterin impairs gastrulation movements and cell rearrangements

(A-C) Maximum projection of time series from a time-lapse experiment of a GFP electroporated embryo treated with the cell division inhibitor Aminopterin. The last ten time points have been pseudo-colored in red. **(A'-C')** Cartoon depicting the trajectories of a few cells shown in A-C). The position of the primitive streak is indicated by a red dotted line. (**D)** First time point of a 1hour time-lapse experiments of an Aminopterin treated embryo, showing the region used for

junction transition analyses in **(D'). (D')** Cartoon schematizing transitions that each cell-cell junction will undergo over 1h as explained in the legend of Figure2K. **(E and E')** Time series of an Aminopterin treated embryo on which stripes of cells have been artificially labelled (in blue, green and red) to reveal the effect on cell organization between (t0) **(E)** and t+100min **(E').** Note that in Aminopterin treated embryos, the cellular organization remains almost unchanged after 100min.

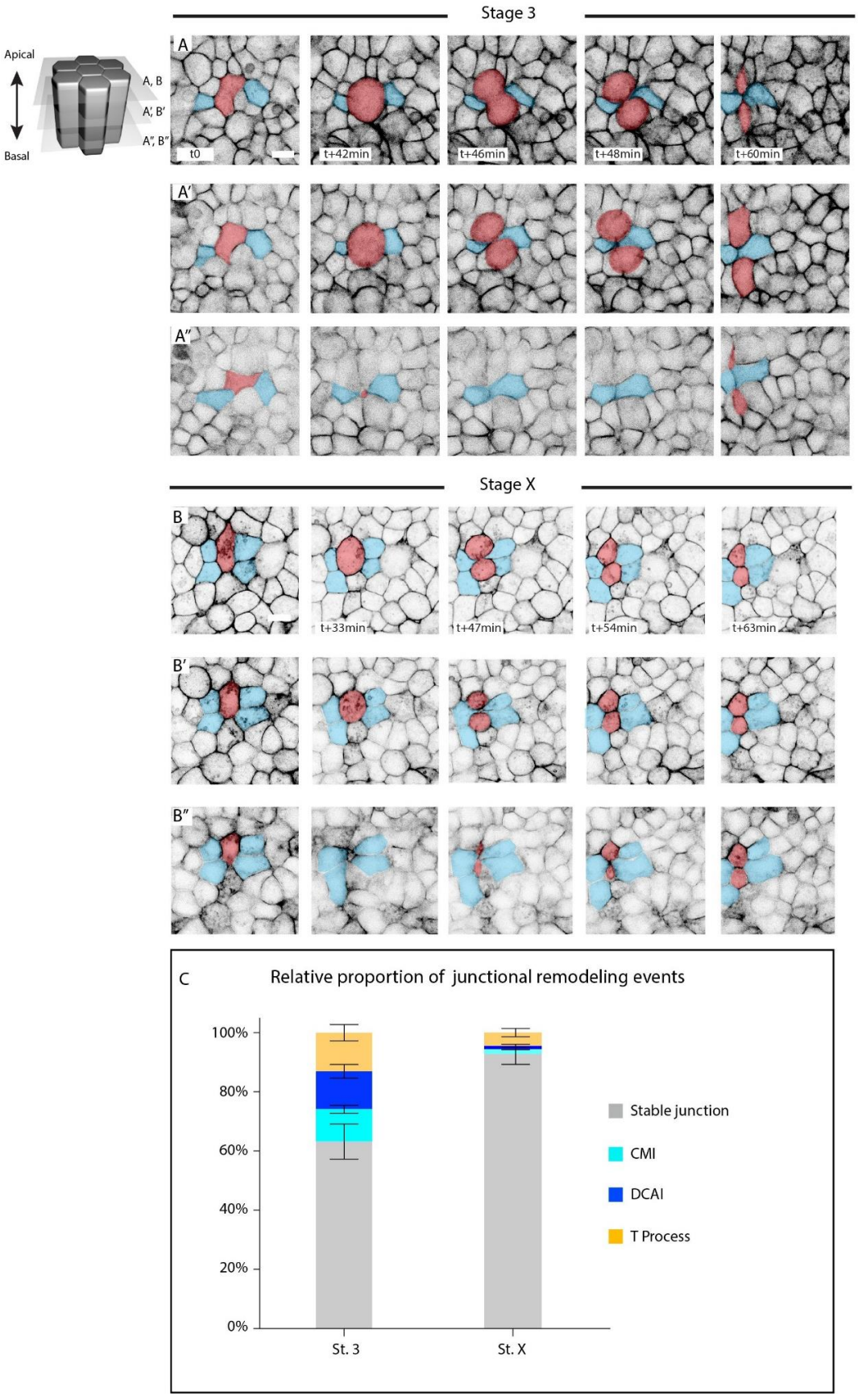
Stage 3
Apical
Basal
A, B
A′, B′
A″, B″
A
A′
A″
t0
t+42min
t+46min
t+48min
t+60min
Stage X
B
B′
B″
t+33min
t+47min
t+54min
t+63min
C
Relative proportion of junctional remodeling events
100%
80%
60%
40%
20%
0%
St. 3
St. X
Stable junction
CMI
DCAI
T Process

Figure S2, related to figure 4. Spatiotemporal characterization of cell division mediated intercalations at stage 3 and daughter-daughter cell junction formation at stage X.
(A and B) Time series of WT stage 3 (A) and stage X (B) memGFP transgenic embryo acquired with a 2-photon microscope at three different z-positions: sub apical (A, B), medial (A', B') and basal (A", B"). A dividing cell and its neighbors have been highlighted in red and blue respectively. At stage 3 (A) , as the cell rounds up, neighbors first establish a novel contact basally (A'') which then progresses apically, as cytokinesis proceeds and eventually expands in the plane of the epithelium, whereas at stage X (B) intercalation never takes place basally. Scale bar is 10μm.
(C) Quantifications of the relative proportion of stable, Cytokinesis Mediated Intercalations (CMI), Daughter Cell Associated Intercalations (DCAI) and T processes in stage X and stage 3 memGFP embryos.
Scale bar is 10μm.

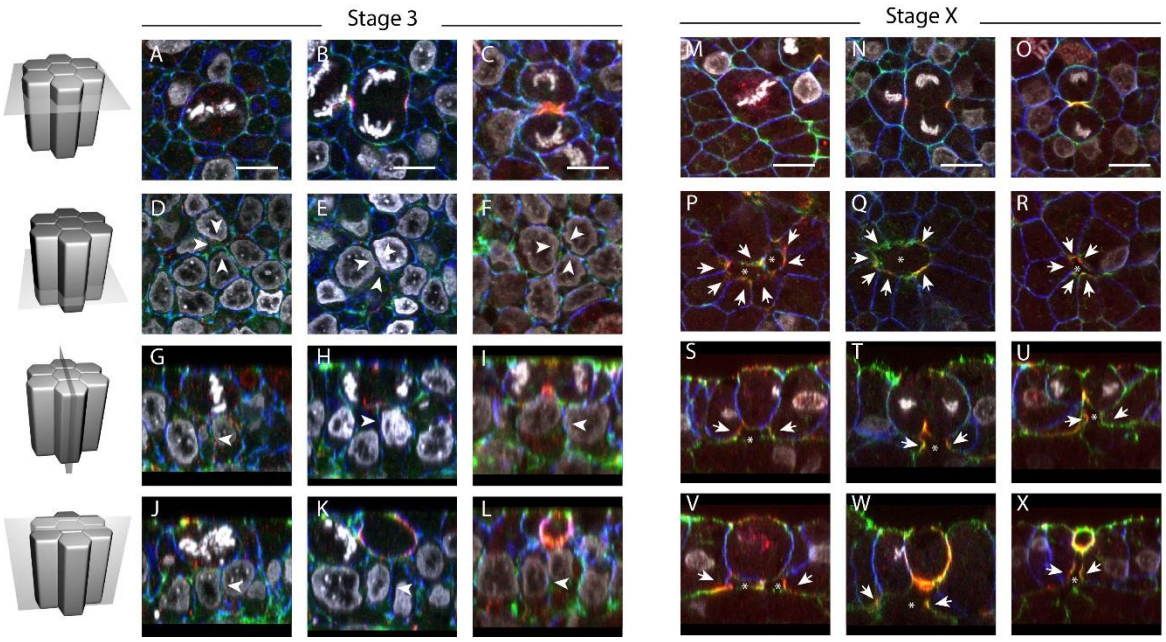

Figure S3, related to Figure 4. Basolateral accumulation of F-actin and pMyosin in cells neighboring a dividing cell at stage X.

(A-X) Confocal ortho-slices of stage 3 (A-L) and stage X (M-X) whole mount embryos stained with Phalloidin, pMyosin and E-Cadherin antibodies showing dividing cells and their neighbors at different steps of the division process. White arrows point at F-actin and pMyosin accumulation, asterisks show free-contact cell interfaces and arrowheads point at basal E-cadherin junctions.

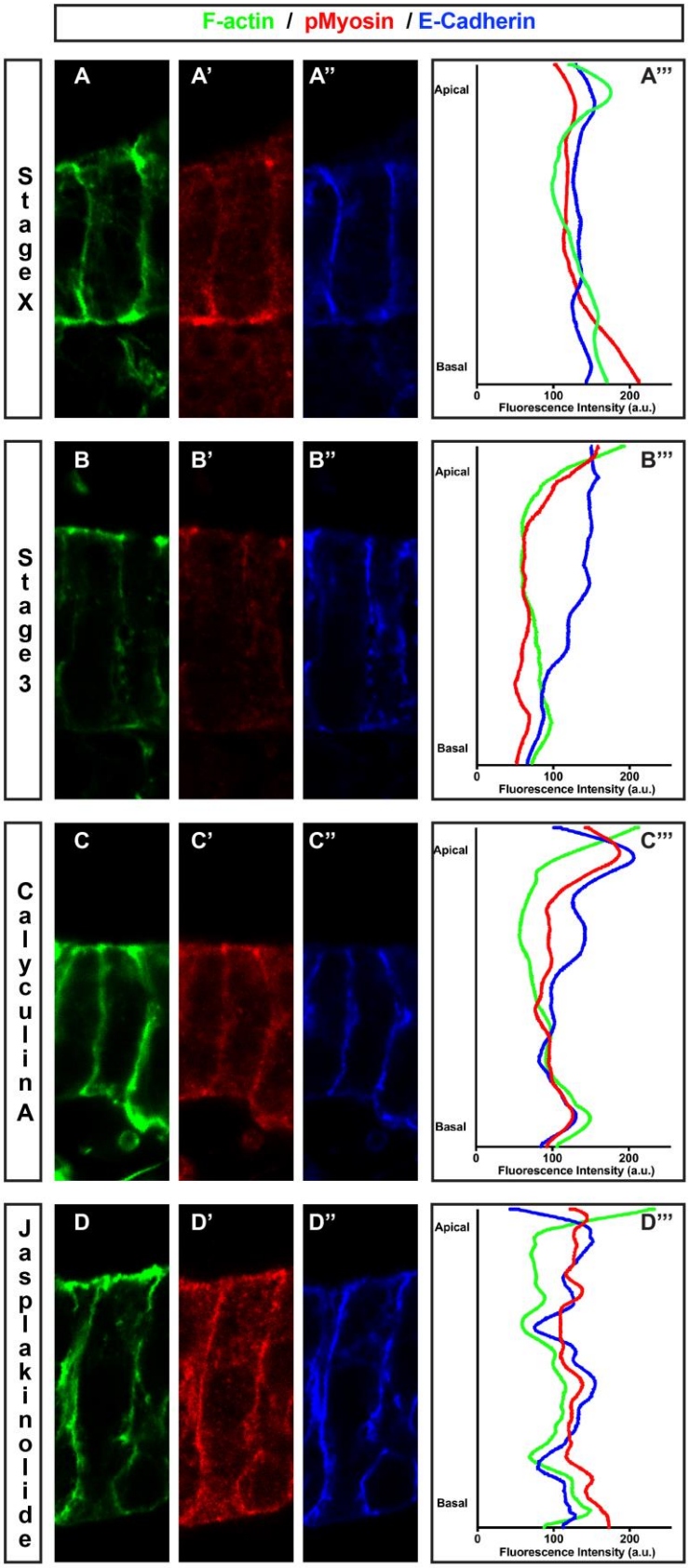
F-actin / pMyosin / E-Cadherin
Stage X
A
A'
A''
A'''
Apical
Basal
0
100
200
Fluorescence Intensity (a.u.)
Stage 3
B
B'
B''
B'''
Apical
Basal
0
100
200
Fluorescence Intensity (a.u.)
Calyculin A
C
C'
C''
C'''
Apical
Basal
0
100
200
Fluorescence Intensity (a.u.)
Jasplakinolide
D
D'
D''
D'''
Apical
Basal
0
100
200
Fluorescence Intensity (a.u.)

Figure S4, Figure S4, related to Figure 4 and 5. pMyosin and F-actin show different intensity profile along the apicobasal axis between Stage X, Calyculin A and Jasplakinolide treated embryos and Stage 3 embryos.
(A-D, A'-D' and A''-D'') Immunofluorescence using Phalloidin (A-D), pMyosin (A'-D') and E-Cadherin (A''- D'') antibodies in a stage X (A-A''), stage 3 (B-B''), Calyculin A treated (C-C'') and Jasplakinolide treated (D-D'') embryo.
(A'''- D''') Fluorescence intensity profile of Phalloidin (green), pMyosin (red) and E-Cadherin (blue) along the apico basal axis of cell-cell interfaces (n=7 junctions per condition). Cell-cell interfaces with different lengths were linearly normalised and the obtained curves were smoothened using a 2nd order polynomial Savitzky-Golay filter. Note that in stage 3 embryos, pMyosin and F-actin are mostly expressed apically rather than basolaterally contrary to stage X, Calyculin A and Jasplakinolide treated embryos.

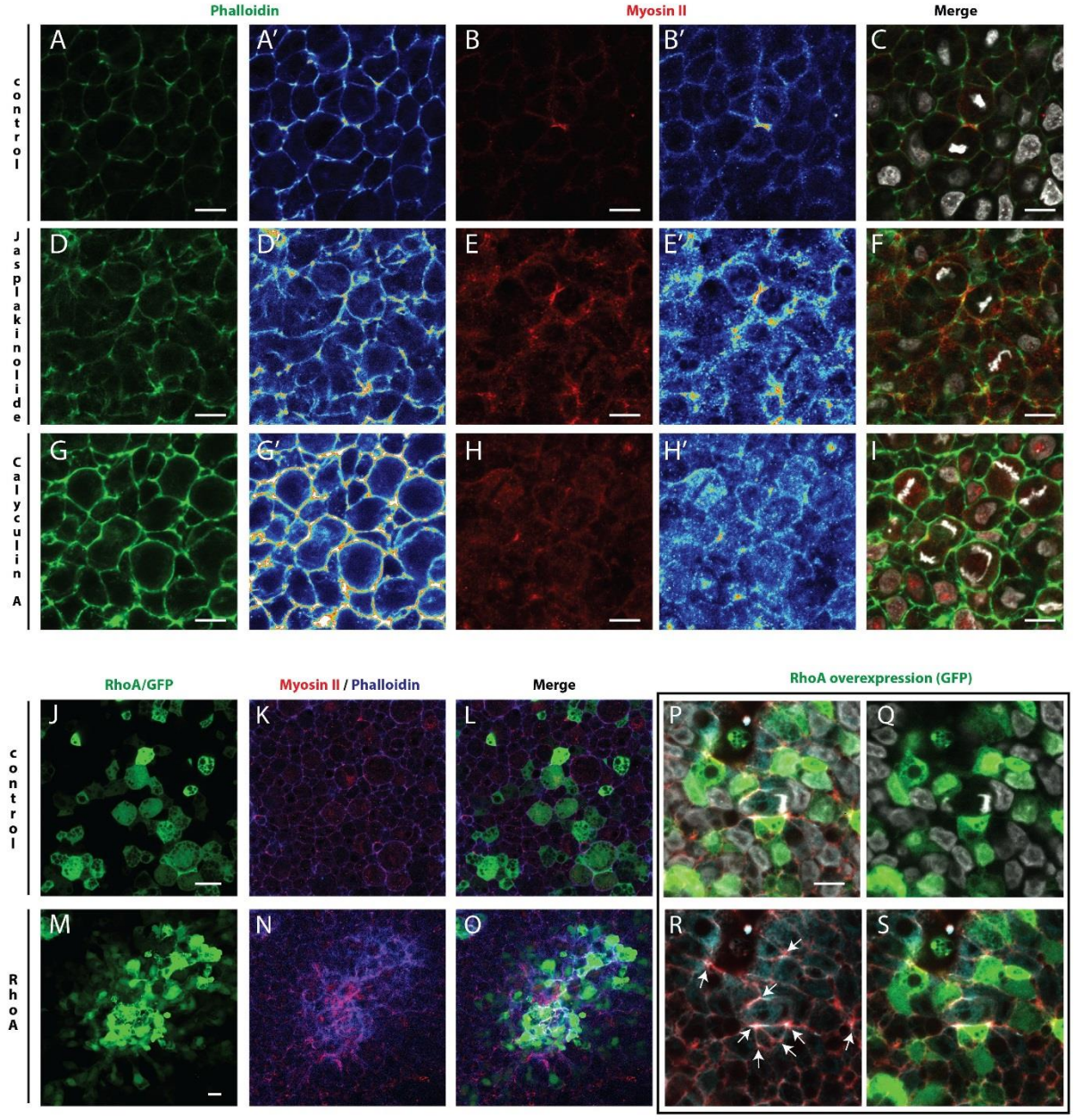

Figure S5, related to Figure 4 and 5. Jasplakinolide, Calyculin A treatment and RhoA/GFP electroporation lead to an increase in Myosin and F-actin levels

(A-I) Immunofluorescence of a control (A-C), Jasplakinolide (D-F) and Calyculin A (F-I) treated embryo using Phalloidin to reveal F-actin (green) and Myosin II antibody (red) and Hoechst in (white). Heat maps of Phalloidin (A', D', G') and Myosin (B', E', H') stainings where low levels correspond to black and high levels to white. Note how both stainings show overall increased levels in Jasplakinolide and Calyculin A conditions. **(J-L)** Immunofluorescence of a GFP **(J, K,**

L) or RhoA/GFP **(M, N , O)** electroporated embryo using Phalloidin in blue and Myosin II antibody in red and GFP antibody in green **.** Note the increased levels of MyosinII and F-actin within the RhoA/GFP electroporated area

(P-S) Higher magnification of a RhoA electroporated region, highlighting increased actomyosin levels in immediate neighbors ($RhoA^{+}$) of a dividing cell ($RhoA/GFP^{-}$**).** GFP is in green, F-actin in red, myosin in blue and Hoechst in white**.** Arrowheads highlight junctions with increased levels of F-actin and Myosin II. Scale bar is 10μm.

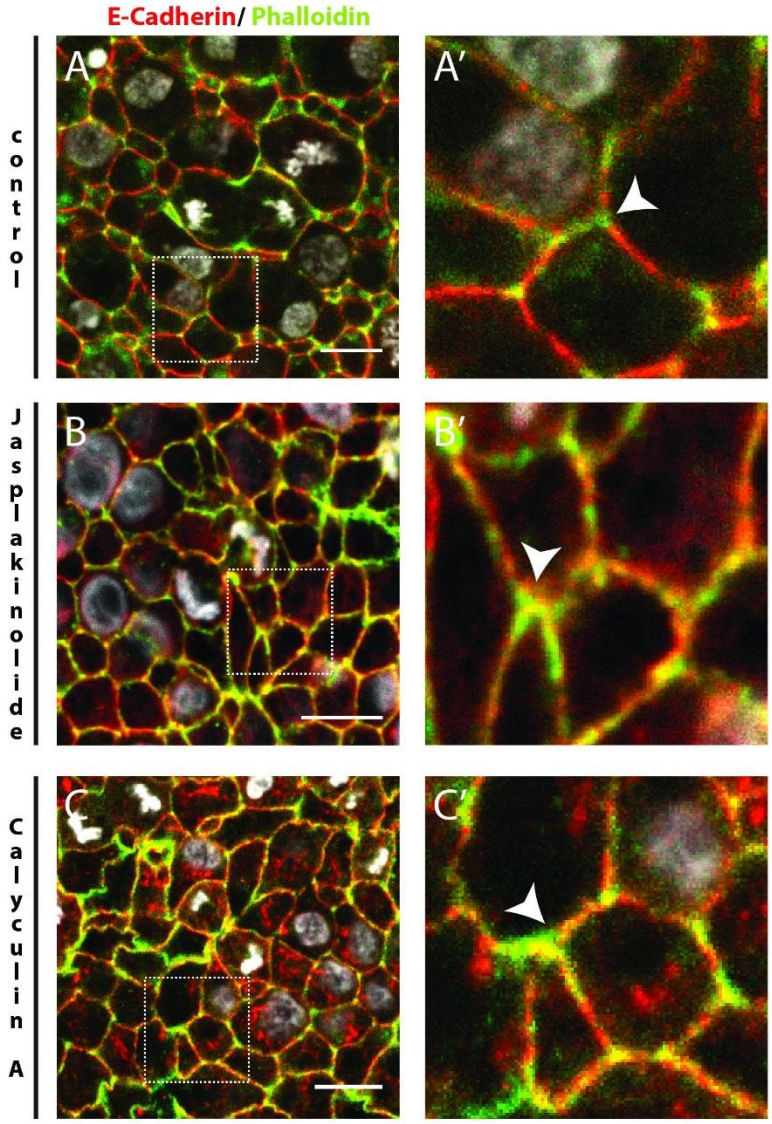

Figure S6, related to Figure 6. Jasplakinolide and Calyculin A treatments increase E-Cadherin and F-actin association.

(A-C) Immunofluorescence using E-Cadherin antibody (red) and Phalloidin (green) in a control (A), Jasplakinolide (B) and Calyculin A (C) treated embryos. (A'-C') Higher magnification of the boxed area in (A-C**)**. Arrowheads point at increased E-Cadherin and F-actin association at cell-cell junctions in cells neighboring a dividing cell compared to control (arrow). Scale bar is 10μm.

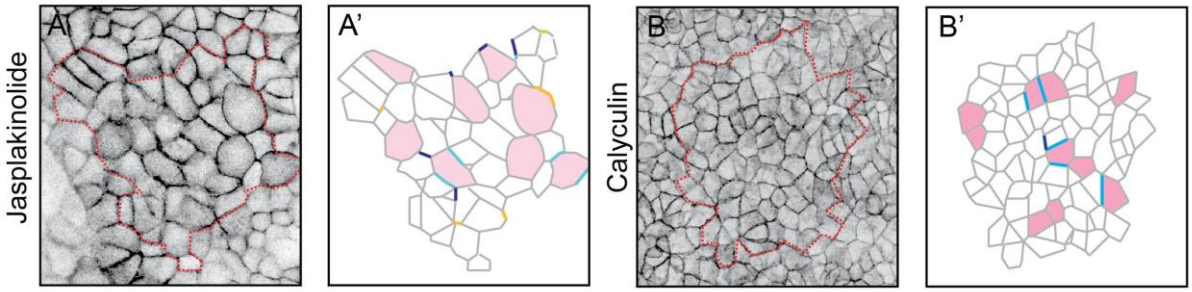

Figure S7, related to figure 6. Jasplakinolide and Calyculin A treatments stabilize epithelial organization

(A and B) First time point of a 1hour time-lapse experiments of memGFP embryos treated with Jasplakinolide (A) and Calyculin A (B), showing the region used for junction transition analyses in (A' and B'). (A', B') Cartoon schematizing transitions that each cell-cell junction will undergo over 1h in the region boxed in (A, B) respectively. Same color code as in Figure 2F is used.

Supplemental Movies Legends

Movie S1. Daughter cells separate upon division as gastrulation movements take place, related to Figure 1.
Left Panel: 3h time-lapse experiment of a stage 3+ GFP-electroporated chick embryo, using a 10x objective on a confocal microscope, revealing the symmetrical and rotational flow of cells.
Middle panel: 25-minute time-lapse experiment of a GFP electroporated chick embryo using a 40x objective.
Right panel: 30-minute time-lapse experiment of a stage 3 memGFP transgenic chick embryo, using a 40x objective; cells undergoing division are pseudo-colored at the beginning and at the end of the movie to reveal cell intercalation between daughter cells within 30min.

Movie S2. Cell division progressively promote rearrangements between stage X and 3, related to Figure 1.
1st segment (0-6s): Movies on the right show regions typically acquired and analyzed in memGFP stage X (upper panel) and stage 3 embryos (lower panel). Movies were acquired with a 40x objective and the tiling stitching module of the confocal microscope. Images on the left show the position of the movies acquired relative to rest of the embryo (acquired with a 10x and the tiling stitching module of the confocal microscope). Colored lines denote cell divisions and their orientation (red lines point a cell divisions which lead to daughter cell juxtaposition, green lines to daughter cells that separate from each other). The last image of the movies is a maximum intensity projection highlighting global tissue flow (memGFP signal) and cell divisions that took place during the 1h time lapse.
2nd segment (6-20s): 60-minute time-lapse experiment of a stage X and 3 memGFP transgenic chick embryo using a 40x objective, in which a dividing cell and its neighbors have been highlighted in red and blue respectively. The memGFP signal is inverted and shown in black. Note that at stage X upon cell division cells do not rearrange whereas at stage 3, light blue colored neighbors intercalate between daughter cells (CMI) and daughter cells intercalate between deep blue colored neighbors (DCAI).

Movie S3. Junctional remodeling and cell rearrangements in Control and Aphidicolin treated embryos, related to Figure 2.
1st segment (0-8s): illustration of junction state assignment (CMI transitions, DCAI, transitions, T transitions, and stable). Note that a minimum number of junctions have been annotated for clarity. On this movie 2CMI, 5DCAI, 1 T1 events are annotated whereas 16 junction remain stable.
2nd segment (8-14s): Example of a time-lapse experiment of a control and aphidicolin treated memGFP transgenic embryo used to characterize the evolution of each cell-cell junction in the boxed region (in red) over the course of 1h. Note that in Aphidicolin, cells only undergo T1

(junction remodeling independent of cell division) and T2 (extrusion from the epithelial sheet) transitions as cells do not divide.
3rd segment (14-24s): Time-lapse experiment of a WT memGFP transgenic chick embryo using a 40x objective. Stripes of cells and their progeny have been artificially labeled (red, green and blue) at the beginning of the movie and tracked for 100min to reveal the effect of cell rearrangements on cell organization. Note that in the control, after 100min the striped pattern is not recognizable, as cells have widely dispersed whereas in aphidicolin treated embryos the striped pattern is almost unchanged, revealing the dramatic effect of cell division on cell rearrangements.

Movie S4. Cell movements in Aphidicolin treated embryos, related to Figure 2.
3h time-lapse experiment of an Aphidicolin treated, GFP electroporated chick embryo between stage HH3 and HH4 using a 10x objective. 1h after the beginning of the movie the Polonaise movements become disrupted and cells move towards the primitive streak of the embryo.

Movie S5. Isolation of epithelial region using laser microdissection, related to Figure 3.
Time lapse experiment showing laser micro-dissection of an epithelial region lateral to the primitive streak of a memGFP stage 3 embryo and subsequent imaging. UV- microdissection as well as imaging were performed using a 10x objective. Colored lines denote cell divisions (red lines point a cell divisions which lead to daughter cell juxtaposition, green lines to daughter cells that separate from each other).The last image of the movie is a maximum intensity projection highlighting global tissue flow (memGFP signal) and cell divisions that took place during the 1h time lapse. Scale bar is 100μm.

Movie S6. Increased myosin and F-actin stability prevents cell division mediated rearrangements, related to Figure 6.
Time-lapse experiments of Calyculin A (left panel), Jasplakinolide (middle panel) treated memGFP transgenic chick embryos and RhoA electroporated embryo (right panel) cell divisions using a 40x objective. Neighbors of dividing cell (red asterisk) fail to intercalate between the resulting daughters and a daughter-daughter cell junction forms.